



Mapping Solar System chaos with the Geological Orrery

Paul E. Olsen^{a,1}, Jacques Laskar^b, Dennis V. Kent^{a,c}, Sean T. Kinney^a, David J. Reynolds^d, Jingeng Sha^e, and Jessica H. Whiteside^f

^aLamont-Doherty Earth Observatory of Columbia University, Palisades, NY 10968; ^bObservatoire de Paris, Paris Sciences & Lettres, Research University, Sorbonne Université, 75006 Paris, France; ^cEarth and Planetary Sciences, Rutgers University, Piscataway, NJ 08854; ^dExxonMobil Exploration Company, Houston, TX 77060; ^eState Key Laboratory of Palaeobiology and Stratigraphy, Nanjing Institute of Geology and Paleontology and Center for Excellence in Life and Paleoenvironment, 210008 Nanjing, China; and ^fOcean and Earth Science, National Oceanography Centre, University of Southampton, SO14 3ZH Southampton, United Kingdom

Contributed by Paul E. Olsen, January 16, 2019 (sent for review August 13, 2018; reviewed by James W. Head and Linda A. Hinnov)

The Geological Orrery is a network of geological records of orbitally paced climate designed to address the inherent limitations of solutions for planetary orbits beyond 60 million years ago due to the chaotic nature of Solar System motion. We use results from two scientific coring experiments in Early Mesozoic continental strata: the Newark Basin Coring Project and the Colorado Plateau Coring Project. We precisely and accurately resolve the secular fundamental frequencies of precession of perihelion of the inner planets and Jupiter for the Late Triassic and Early Jurassic epochs (223–199 million years ago) using the lacustrine record of orbital pacing tuned only to one frequency (1/405,000 years) as a geological interferometer. Excepting Jupiter's, these frequencies differ significantly from present values as determined using three independent techniques yielding practically the same results. Estimates for the precession of perihelion of the inner planets are robust, reflecting a zircon U-Pb-based age model and internal checks based on the overdetermined origins of the geologically measured frequencies. Furthermore, although not indicative of a correct solution, one numerical solution closely matches the Geological Orrery, with a very low probability of being due to chance. To determine the secular fundamental frequencies of the precession of the nodes of the planets and the important secular resonances with the precession of perihelion, a contemporaneous high-latitude geological archive recording obliquity pacing of climate is needed. These results form a proof of concept of the Geological Orrery and lay out an empirical framework to map the chaotic evolution of the Solar System.

Solar System | orbital dynamics | Milankovitch | chaos | Triassic–Jurassic

In the introduction of his 1812 treatise on probability, Pierre-Simon de Laplace (1) envisioned the possibility of modeling the whole universe in a single equation (the gravitational laws). Using only knowledge of the present initial conditions, one could recover all of the past and predict all of the future. However, this paradigm of determinism does not apply to the Solar System. The validity of the solutions of Solar System gravitational models is constrained to about 0–60 Ma not only because of inherent limitations in the determination of initial conditions and parameters of the model but more fundamentally, because of the chaotic nature of the system for which initially close solutions diverge exponentially, in fact multiplying the uncertainties by a factor of 10 every 10 My (2, 3). Although there has been much recent progress, the powerful constraint imposed by chaos, at several levels, means that it is hopeless to attempt to retrace the precise history of the Solar System from only knowledge of the present as has been done until now. Conversely, geological data can constrain the astronomical solution back in time, thus allowing us to go beyond the horizon of predictability of the system. Geological data recording climate variations modulated by celestial mechanics potentially provide an empirical realm to test astronomical solutions that must conform to the past. Geological data from within the last 60 My seem to agree with astronomical solutions (4, 5) but provide little information on the Solar System beyond what is already known. The fundamental challenge is to find empirical data well beyond 60 Ma to provide anchors for extending the astronomical

solutions, but this quest has been hampered by a lack of records with both sufficient temporal scope and independent age control. To circumvent the limitations of most geological data, we have developed an experimental system that uses a plexus of highly resolved data from multiple temporally correlative and complementary records termed “The Geological Orrery,” named after the mechanical planetaria—Orreries—of the 18th century from the fourth Earl of Orrery, Charles Boyle (6), and the “Digital Orrery,” a dedicated parallel-processing computer that was constructed to investigate the long-term motion of the Solar System that numerically confirmed its chaotic nature (7, 8). The Geological Orrery provides a procedure to fully map the actual gravitational history of the last ~250 My of the Solar System and beyond, allowing reliable filtering and modification of astronomical solutions.

To a first approximation, the orbital planes of the planets are slowly deformed by the gravitational forces of the other bodies in the Solar System in a quasiperiodic way that can be decomposed into a series of secular fundamental frequencies representing roughly each planet’s contribution to the deformation of the orbits. These motions can be described in terms of the precession of perihelion in the orbital plane (g_i frequencies) and the precession of the orbital plane in space represented by the precession of the node (s_i frequencies). Differences of these secular frequencies of precession of perihelion g_i yield the “eccentricity cycles” familiar to paleoclimatologists, and the sums of the g_i frequencies with Earth’s axial precession constant, p , yield the “climatic precession” frequencies, today averaging about 21 ky (Table 1). Similarly, the difference frequencies of the secular fundamental frequencies of precession

Significance

The Solar System is chaotic, and precise solutions for the motions of the planets are limited to about 60 million years. Using a network of coring experiments that we call the Geological Orrery (after 18th century planetaria), we recover precise and accurate values for the precession of the perihelion of the inner planets from 223- to 199-million-year-old tropical lake sediments, circumventing the problem of Solar System chaos. Extension of the Geological Orrery from 60 million years ago to the whole Mesozoic and beyond would provide an empirical realm to constrain models of Solar System evolution, further test General Relativity and its alternatives, constrain the existence of additional past planets, and provide further tests of gravitational models.

Author contributions: P.E.O., D.V.K., J.S., and J.H.W. designed research; P.E.O., J.L., D.V.K., D.J.R., and J.H.W. performed research; P.E.O., J.L., D.V.K., S.T.K., D.J.R., and J.H.W. analyzed data; and P.E.O., J.L., D.V.K., S.T.K., and J.H.W. wrote the paper.

Reviewers: J.W.H., Brown University; and L.A.H., George Mason University.

The authors declare no conflict of interest.

Published under the PNAS license.

¹To whom correspondence should be addressed. Email: polsen@ldeo.columbia.edu.

This article contains supporting information online at www.pnas.org/lookup/suppl/doi:10.1073/pnas.1813901116/-DCSupplemental.

of the orbital nodes s_i yield the orbital inclination frequencies, and the sums of the s_i frequencies with p yield the familiar obliquity periods today near 41 ky.

Here, we use the Geological Orrery to precisely determine the secular fundamental frequencies of the precession of perihelion of the inner planets and Jupiter from 199 to 220 Ma using climate proxy and geochronologic results from two major scientific coring experiments: (*i*) the Newark Basin Coring Project (NBCP) (9) that forms the basis of the Newark–Hartford Astrochronostatigraphic Polarity Timescale (NH APTS) (10) along with data from the adjacent Hartford Basin (*SI Appendix*) and (*ii*) the Colorado Plateau Coring Project (CPCP–1) (11, 12) (Fig. 1 and *SI Appendix*, Fig. S6 and Table S1).

The NBCP experiment collected seven ~1,000-m continuous cores and core holes in lacustrine to fluvial rift basin strata of the Newark Basin spanning most of the Late Triassic and the earliest Jurassic, which together with additional core and outcrop data (13–15) (*SI Appendix*, Figs. S1 and S6, and Table S1), tested the permeating nature of orbital pacing of lake depth in the paleotropics (0° – 21° N) (16) through the lacustrine part of the section, previously inferred from scarce and discontinuous outcrops (17–19). Global correlation is achieved through 66 geomagnetic polarity intervals pinned in time by zircon chemical abrasion isotope dilution thermal ionization mass spectrometry (CA-ID-TIMS) U–Pb dates from three lava flow formations interbedded in the very latest Triassic and earliest Jurassic age part of the sequence (20, 21). Using largely a facies classification and a color scale, the NBCP experiment (19) supported the hypothesis that the rift lake depth was paced by orbital cycles, including a full range of climatic precession-related cycles. These include the ~20-ky precessional and the ~100- and 405-ky orbital eccentricity cycles with the latter and its mappable geological equivalent termed the McLaughlin Cycle (Table 1), then being used to tune the entire lacustrine part of the composite Newark–Hartford record (22). This, in turn, allowed the Triassic values of the secular fundamental frequencies of the precession of perihelion for Mercury (g1), Venus (g2), Earth (g3), and Mars (g4) (Table 1) to be roughly estimated (22). The tuned data also revealed even longer-period “Grand Cycles” (23) (Table 1), including one with a period of ~1.7 My identified as the Mars–Earth cycle (g4 – g3) that today has a value of ~2.4 My (5), the difference being attributed to chaotic diffusion in the behavior of the Solar System. However, these results lacked independent age control, allowing the possibility that hiatuses invisible to spectral analysis compromise both the timescale and the apparent eccentricity periodicities longer than 405 ky (24–27).

A major goal of the CPCP–1 experiment in the Triassic Chinle Formation in Petrified Forest National Park in Arizona was to provide an independent zircon U–Pb age-constrained paleomagnetic polarity stratigraphy that could be correlated to and test the NH APTS and the application of orbital theory on which it is based (11). CPCP–1 validated the NH APTS interval from ~210 to 215 Ma and implicitly validated the age model for the younger interval bounded by zircon CA-ID-TIMS U–Pb dates from Newark Basin lavas for ~600 ky around ~201 Ma (21), making an independently dated sequence extending from ~201 to 215 Ma in total. These geochronological data validate the NH APTS and provide direct dating of the 405-ky cycle at around 215 Ma (12) (*SI Appendix*, Fig. S7 and Table S2), and they provide the needed age control for examining Triassic–Early Jurassic orbital frequencies in the Newark–Hartford dataset and permit direct comparison with Neogene and Quaternary marine data.

Newark–Hartford Composite Results

The newly compiled Newark–Hartford dataset consists of four major depth series: depth rank (sedimentary facies related to water depth) and color from the recovered cores and down-hole sonic velocity and natural gamma radiation measurements providing instrumental complementary data (*SI Appendix*, Figs. S2 and S6). Data from cores and outcrops from the Newark and Hartford Basins allow seamless extension of the sequence into the Early Jurassic (Hettangian and Early Sinemurian) (12) (*SI Appendix*, Figs. S3–S6).

Wavelet spectra of these four depth series show similar patterns of periodicities in the depth domain with all of the thickness periodicities changing in frequency simultaneously (Fig. 2 and *SI Appendix*, Fig. S6), reflecting variations in accumulation rate. The most prominent frequency through most of the spectrum reflects the lithologically based McLaughlin Cycle, an expression of the 405-ky orbital eccentricity cycle (Table 2), which provided the basis for time calibration of the NH APTS (10). The zircon CA-ID-TIMS U–Pb dates from the Newark Basin lava flow formations and related intrusions show a pronounced (nearly an order of magnitude) (*SI Appendix*, Figs. S6 and S11) increase in accumulation rate at the beginning of the Central Atlantic Magmatic Province (CAMP) event (Fig. 2), above which the thickness frequencies correspondingly shift to much lower values in agreement with the visual observation of the increased thickness of the McLaughlin Cycles (13–15). The borehole geophysical data are complementary to the depth rank data, especially where the latter has reduced variability as shown by both wavelet and Multitaper Method (MTM) spectral analysis

Table 1. Cycle nomenclature and origins of the climatic precession and eccentricity from the secular fundamental frequencies

Named lithological expression of cycles*	Description	Argument	Periods and informal names of Milankovitch or orbital cycle with today's period [†]
Van Houten cycle	Precession frequency of Earth (p) + secular frequency of precession of perihelion of Mercury, Venus...	$p + g1, p + g2, p + g3, p + g4, p + g5$	~21 ky (average 21.5 ky); 23.2-, 22.4-, 19.2-, 19.0-, 23.8-ky climatic precession
Short modulating cycle	Secular frequencies of precession of perihelion of Mars – that of Jupiter, etc.	$g4 - g5, g3 - g2, g4 - g2, g3 - g2$	~100 ky (average 112.1 ky); 94.9-, 98.9-, 123.9-, 130.7-ky short orbital eccentricity cycles
McLaughlin cycle	Venus (g2) – Jupiter (g5)	$g2 - g5$	405-ky long orbital eccentricity Grand Cycle
None	Venus (g2) – Mercury (g1)	$g2 - g1$	696-ky Grand Cycle
None	Mercury (g1) – Jupiter (g5)	$g1 - g5$	973-ky Grand Cycle
Long modulating cycle	Mars (g4) – Earth (g3)	$g4 - g3$	2,365-ky Grand Cycle

*From ref. 9.

[†]Using the g1–g5 values from ref. 5, table 6 and p from refs. 29 and 33, table 1.

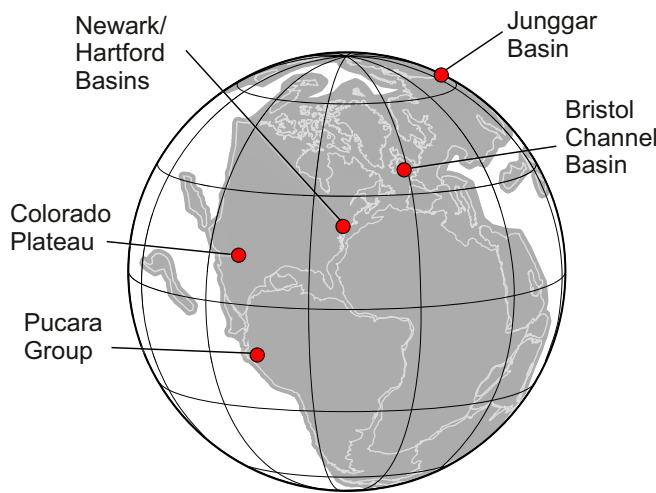


Fig. 1. Map of Pangea at ~ 200 Ma with locations discussed in text.

(Fig. 3 and Fig. 5). MTM analysis of X-ray fluorescence chemical data yields similar results on a subset of the thickness data (*SI Appendix*, Figs. S8 and S9). We regard this as a powerful verification that the main periodicities can be easily seen in all of the depth series by visual inspection without any tuning or non-uniform age model (Fig. 2).

We convert the data from the core depth domain to the time domain with minimal modification using a simple model based on U-Pb dates imported from CPCP-1 via magnetostratigraphy and the lava flows within the section. This yields a spectrum with approximately the expected orbital periodicities (Fig. 4). A prominent cycle at ~ 405 ky is present. By filtering the core depth series in this range to the thickness of this cycle (*SI Appendix*, Fig. S7 and Tables S2 and S3), we can determine its period without having to explicitly identify specific lithological McLaughlin Cycles as was done in ref. 12, which confirms the later results with different methods yielding a periodicity of 398 ± 12 ky using all of the dates and 410 ± 02 ky using only the three CPCP-1 dates in stratigraphic order and the Newark Basin CAMP dates (*SI Appendix*, Fig. S7 and Table S3). Therefore, regardless of the counting methodology, these results are indistinguishable from the 405-ky periodicity predicted to be stable over this time interval (5, 12).

Minimally tuned to the 405-ky periodicity, the wavelet spectra show that all of the frequencies seen in the depth domain are now aligned, and the datasets can be directly compared with the spectrum solution for the later Neogene plus Quaternary (Fig. 5 and *SI Appendix*, Figs. S10 and S12). Visual inspection of the wavelet spectra shows overall agreement in pattern in the high-power periods, except for those longer than 405 ky. In particular, the apparent homolog of the 2.4-My period in the Neogene plus Quaternary wavelet spectrum is distinctly offset to a shorter period of ~ 1.7 My ascribed to the Mars-Earth orbital eccentricity Grand Cycle ($g_4 - g_3$) (Table 2) when it was first measured (22, 23). The 1.7-My cycle is not visible in the NBCP

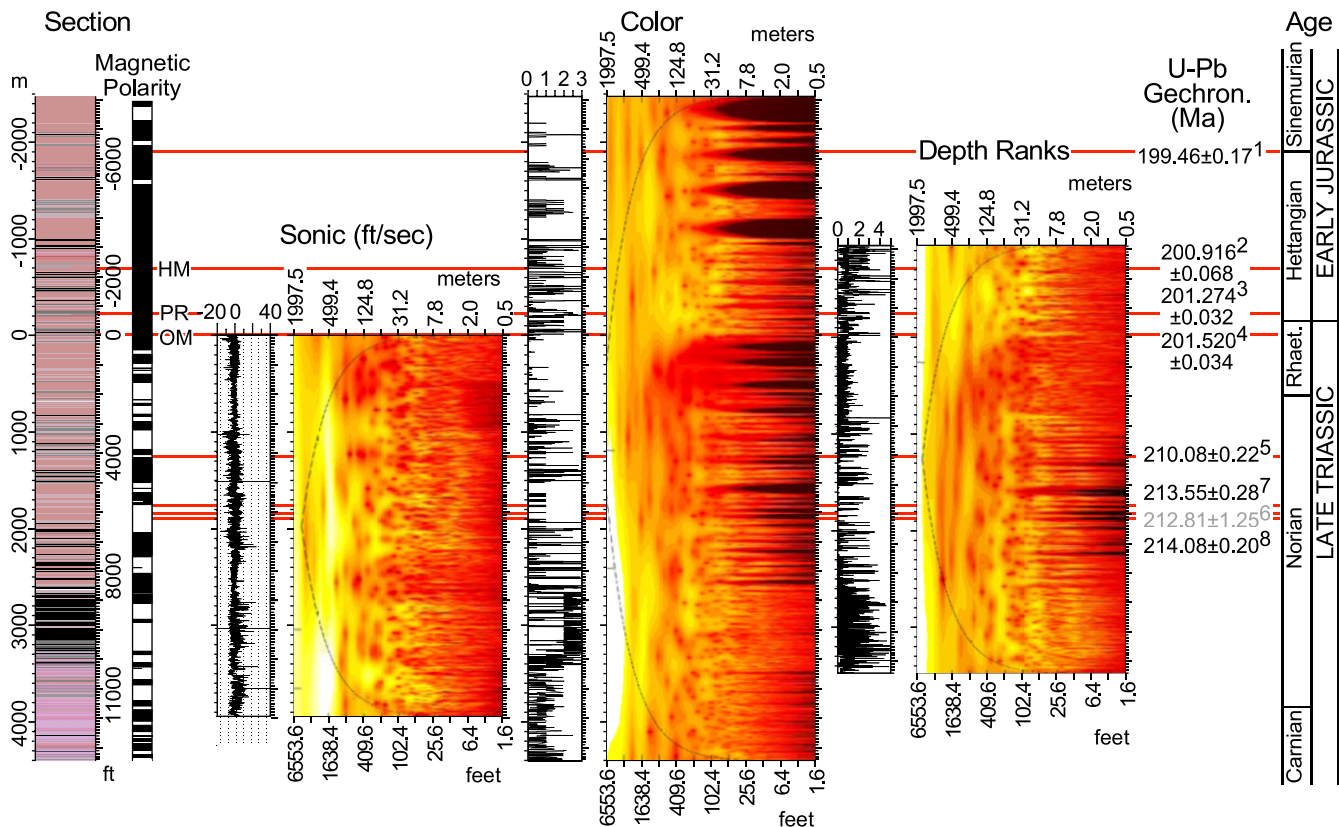


Fig. 2. Untuned Newark-Hartford wavelet spectra from core, holes, and outcrops (*SI Appendix*, Fig. S1 and Table S1). Crucial are the demonstrable and simultaneous shifts in all thickness periods, particularly pronounced in the lower two-thirds of the spectra. There is nearly an order of magnitude increase in accumulation rate above the lowest Basalt [Orange Mt. Basalt (Talcott Basalt in Hartford Basin) (OM)] at 0 m. Red horizontal lines mark positions of the lava flow formations of the CAMP. Zircon U-Pb CA-ID-TIMS ages are as follows: 1, based on paleomagnetic correlation to the Bristol Channel Basin Hettangian-Sinemurian Boundary at Global Boundary Stratotype Section and Point (GSSP) (43, 44) and then to the Pucara Group via ammonite biostratigraphy (46, 47); 2, Butner intrusion related to Hook Mt. Basalt (HM) (21); 3, Preakness Basalt [Holyoke Basalt in Hartford Basin (PR)] (21); 4, Palisade Sill feeder to OM (21); and 5–8, Chinle Formation (12).

Table 2. Periods of the different arguments in the Newark–Hartford data using MTM analysis, FA, and corresponding values in the FA of the La2010d* and La2010a solutions (5) for Earth’s eccentricity (SI Appendix, Table S4)

Row	Argument (frequency)	MTM period (ky)	FA [†] period (ky)	La2010d* ^{‡,§} period (ky)	La2010a ^{†,§} period (ky)
1	g4 – g3	1,724.63	1,747.65	1,793.04	2,368.95
2	g1 – g5	923.04	923.16	957.56	967.42
3	g2 – g1	720.18	719.05	704.98	697.63
4	(g2 – g5) – (g4 – g3)	537.18	527.56	515.09	489.37
5	g2 – g5	405.17	404.97	404.58	405.63
6	(g2 – g5) + (g4 – g3)	336.53	335.13	330.08	346.42
7	g3 – g2	132.53	132.17	132.58	130.71
8	g4 – g2	122.96	123.08	123.47	123.88
9	g3 – g5	99.83	99.78	99.86	98.85
10	g4 – g5	94.43	94.49	94.62	94.89

[†]All terms are recovered by FA in the 14 terms of larger amplitude (SI Appendix, Table S5), except g1 – g5 and g2 – g5 + (g4 – g3), which are of lower amplitude.

[‡]La2010d* is taken over the interval 209–231 Ma.

[§]La2010a is taken over the interval 0–20 Ma.

geophysical logs because of detrending issues with the six down-hole logs from which the composite logs are assembled (SI Appendix, Figs. S2 and S12). The possibility that the difference between the 1.7-My Triassic Period of g4 – g3 and its present 2.4-My period is due to hiatuses is eliminated by the CPCP-1 and Newark Basin lava flow U-Pb dates (SI Appendix, Fig. S7 and Tables S2 and S3).

Examining the interval between the 405-ky cycle and the 2.4-My cycle in the 0- to 24-Ma wavelet spectra, there are two bands of high power with a “ropy” appearance (Fig. 5 and SI Appendix, Fig. S12). They seem to have their homologs in a similar interval in the depth rank and color wavelet spectra in the Newark–Hartford spectra. These various Grand Cycles seem to correspond to the main terms of the eccentricity orbital solution (refs. 5, figure 5; 28; and 29, table 6) (SI Appendix, Table S4); predicted by combinations of the secular fundamental frequencies (Tables 1–3), these should correspond to the Jupiter–Mercury ($g_5 - g_1 = 1/972.59$ ky) and Venus–Mercury ($g_2 - g_1 = 1/695.65$ ky) cycles (Table 2 and SI Appendix, Table S4). To our knowledge, these have not previously been identified in any geological records. Because they are different in value from modern frequencies, assignment of these bands of spectral power to specific combinations of astronomical parameters raises the question of whether they could reflect geological noise or artifacts.

Secular Fundamental Frequencies of the Solar System

Fortunately, the question of the origin of the cycles in the Newark–Hartford dataset can be convincingly answered using refined Fourier analysis techniques in conjunction with the internal cross-checks afforded by the overdetermined components of the orbitally paced cycles themselves (SI Appendix, Table S7). MTM spectral analysis of the cycles with periods greater than 66 ky previously used for this sequence has been applied again here (Fig. 6, Table 2, and SI Appendix, Table S4). In addition, we have performed an independent analysis adopting a method developed for the quasiperiodic decomposition of the output of numerical integrations of dynamical systems called “Frequency Analysis” (FA) (30, 31) that has been widely used in various domains, including experimental physics (28, 29, 32). FA automatically extracts the frequencies and amplitudes of the periodic components of a signal without the need for manual selection of peaks sorted by decreasing amplitude. We applied FA to the whole Newark–Hartford depth rank dataset (200.65–225.565 Ma) after removing a 2-My running average using the computer code (SI Appendix). The FA results, limited to the 14 main terms (Table 2), are extremely close to the MTM analysis (Table 2 and SI Appendix, Table S4). Thus, we have obtained the same result using three different approaches

(wavelet, MTM, and FA). The FA values will be used henceforth for additional quantitative analysis because of its reduced operator influence.

The MTM and FA analyses of the Newark–Hartford data exhibit striking similarities in the recovered values to periodic components of Earth’s orbital eccentricity in numerical solutions of the past 20 My (compare columns 4 and 6 of Table 2) (e.g., ref. 29, table 6). This is similar to an earlier analysis that predated the independent age model (22). However, the important discrepancies with the past 20 My can now be taken more seriously, the most notable being in the g4 – g3 argument that has a present period of 2.364 My in the solution termed La2010a of ref. 5 but only 1.747 My in the Newark–Hartford data. It was argued in ref. 22 that this was the result of chaotic diffusion in the Solar System. We show here that this conclusion is most likely correct with a very high probability.

To a first approximation, the Solar System orbital motion can be considered quasiperiodic, and its long-term evolution can be represented by periodic terms of only 15 main frequencies: the frequencies g_1, g_2, \dots, g_8 [the secular fundamental frequencies of precession of perihelion of the planets (Mercury, Venus, ... Neptune)] and s_1-s_4 and s_6-s_8 [the secular fundamental frequencies of precession of the nodes of the orbits of the planets (s_5 is not present due to the conservation of angular momentum)]. Here, the secular frequencies are regarded as an average over 20 My. Insolation quantities on Earth are thus expressed in terms of these secular fundamental frequencies and additionally, the precession frequency of the spin axis of the Earth, p (29, 33, 34). In general, the secular fundamental frequencies do not appear directly in the physical variables but only as combinations of the frequencies (Tables 1 and 2 and SI Appendix, Table S4). For example, in Earth’s orbital eccentricity, only differences of the form $g_i - g_j$ are present and eventually, combinations of higher order of the g_i , with a zero sum of the coefficients (29). The largest-amplitude term in the Earth’s orbital eccentricity is the well-known $g_2 - g_5 = 1/405$ -ky periodic term. Although the secular fundamental frequencies cannot be measured directly in sedimentary records due to a lack of resolution, the physical effects appear as the differences of frequencies, and these secular difference frequencies generate long-period beats that can be measured, with even longer periods than the $g_5 - g_2 = 1/405$ -ky term. The geological record can thus be viewed as an interferometer in which the lower, measurable frequencies, the Grand Cycles, can be determined, although the higher frequencies that produce them cannot (Tables 1 and 2 and SI Appendix, Table S5). We thus can derive the secular fundamental frequencies pertaining to the

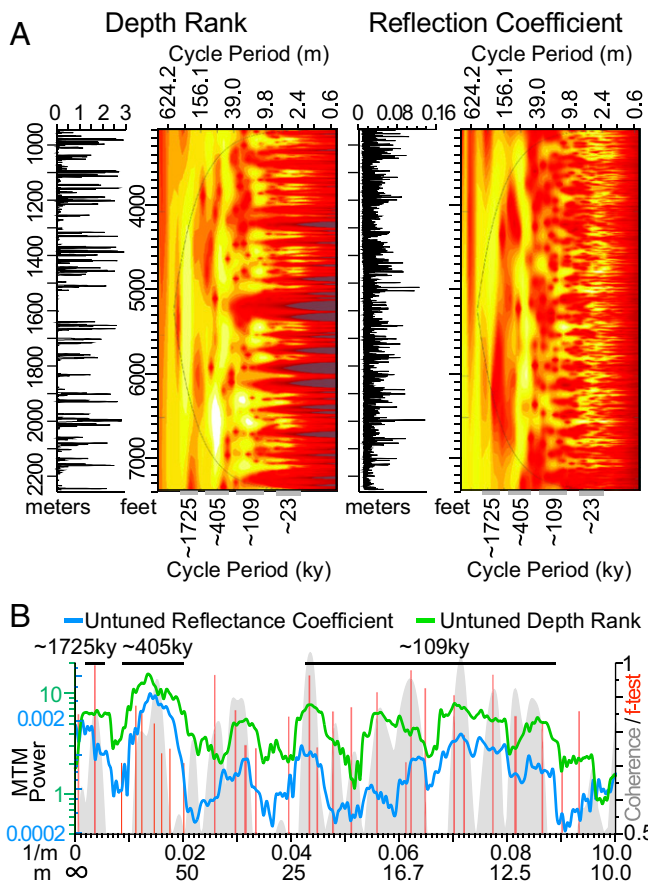


Fig. 3. Comparison between untuned depth rank data from core and reflection coefficient (60) data (derived from borehole sonic velocity and density measurements from Rutgers and Somerset cores and holes of the NBCP; ref. 38) (*SI Appendix*) showing similarity in periods. The interval from ~1,530 to ~1,640 m lacks structure in depth ranks but shows clear periodicities similar to surrounding strata in the reflection coefficient data. (A) Comparison of wavelet spectra showing similar structure and periodicities. (B) MTM spectra of depth rank and reflection coefficient data showing similar cyclicity attributed to orbital eccentricity as well as the “F test” (*f* statistic values greater than 0.7 for both datasets; Analyseries 2.0 default: 6, 4pi tapers) and Blackman-Tukey coherence between the datasets (Analyseries 2.0 default: 30% autocorrelation; 80% confidence level). Note the close correspondence between frequencies with high coherence, high statistical significance, and high power.

precession of perihelion g1 through g4 directly from the geological data untethered from current values.

Chaotic Diffusion

Although over a few million years, the orbital evolution of the Solar System can be approximated by a quasiperiodic motion, as stated above, this is not true extending back in time to 200 Ma, where the chaotic diffusion of the system is noticeable. The main result is a small drift in the values of the secular frequencies of the system (5, 29, 30). This drift is small for individual frequencies, but its effects are greatly amplified in differences of close frequencies (i.e., beat cycles) as in the $g_4 - g_3$ Mars–Earth orbital eccentricity term. The period of this term is at present 2.364 My, while the observed value in the Newark–Hartford data is apparently only 1.747 My (both FA results) (Table 2). Is this possible within the range of the predicted chaotic drift?

To answer this question, we cannot directly integrate the orbital solution back in time starting with the present initial conditions. Indeed, due to the chaotic behavior of the Solar System, the uncertainty in the solutions is multiplied by 10 every 10 My,

and due to the sensitivity of the gravitational system to perturbations of the largest asteroids (minor planets) Ceres and Vesta, it will never be possible to retrieve precisely the planetary orbits beyond about 60 Ma (35). Nevertheless, the problem can be addressed in a probabilistic way by integrating the model beyond that time. While this does not provide the exact path of our Solar System but only a possibility for its past evolution, it does provide a gauge of the reasonableness of the geological data. We thus use 13 orbital solutions of the very precise models termed La2004 of ref. 29 and La2010 of ref. 5 with small variations in the initial conditions compatible with our present knowledge and examine the evolution of the Mars–Earth ($g_4 - g_3$) period from 0 to 250 Ma (Fig. 7A). The output is analyzed using FA with a sliding window of 20 My, with a 1-My offset between each interval (Fig. 7 and *SI Appendix*, Figs. S4 and S6). Among these 13 solutions, 4 of them have a ($g_4 - g_3$) period that goes below 1.75 My, and this is very nearly so for another 4. Thus, finding a 1.75-My value in the geological record in the 200- to 225-Ma time interval is entirely compatible with our best knowledge of Solar System motion.

After this first step, we search for a more quantitative estimate. The solution termed La2010d of ref. 5 comes close to the 1.75-My value in nearly the same time interval as the Newark–Hartford data, and we can consider it our reference solution we term La2010d*. We thus can compare how closely the Newark–Hartford data approximate La2010d* not only for the Mars–Earth ($g_4 - g_3$) cycle but also, for all of the major secular (difference) frequencies for Earth’s orbital eccentricity. Direct comparison of the FA results of La2010d* Earth’s eccentricity (Table 2 and *SI Appendix*, Table S4) with those of the Newark–Hartford data (columns 4 and 5 of Table 2) shows that the values of the periods are very close for all of the leading terms of the analyzed data (*SI Appendix*, Table S5). For a quantitative estimate, we use the frequencies expressed as arcsec per year rather than the period (in years), because they may be combined in a simpler way (Table 3 and *SI Appendix*, Table S4).

Fundamental Secular Frequencies

We can recover the fundamental secular frequencies from the Newark–Hartford data because of the great stability of the outer Solar System, notably Jupiter. The Newark–Hartford data are tuned to the $g_2 - g_5$ Venus–Jupiter 405-ky term, and we expect that FA (and MTM) should recover this value (column 4 of Table 2), which it does. While there is nothing new here, it verifies the consistency of our procedures. In addition, because the outer Solar System is very stable, the g_5 frequency can be considered as a constant over the age of the Earth. The uncertainty in the 405 ky of one cycle in 250 My is due almost entirely to g_2 (5). Indeed, the g_5 value of La2010d*, obtained with FA, is 4.257438 "/y, extremely close to the La2010a value of 4.257482 "/y in ref. 5. With this assumption, supported by theory and computation, we can recover g_1 from $g_1 - g_5$, g_3 from $g_3 - g_5$, g_4 from $g_4 - g_5$, and g_2 from $g_2 - g_5$. For the last, the fact that we find a value close to the La2010a reference value is expected due to the tuning to $g_2 - g_5$ (Table 3). The recovered values for g_1 through g_4 are in column 4 of Table 3. We do not compare these values with the La2010a values but with the ones of La2010d* that should be much closer because this solution has drifted in a similar way due to chaotic diffusion (Fig. 7B). Indeed, the differences reported in column 5 of Table 3 are extremely small.

This should be sufficient to give us great confidence that the signal that we have recovered in the Newark–Hartford data is related to the Earth’s orbital eccentricity, but there is much more that can be recovered. Indeed, in the leading terms provided by FA, there are five additional terms in the FA of the La2010d* eccentricity solution. These terms, $g_4 - g_3$, $g_2 - g_1$, $g_2 - g_5 - (g_4 - g_3)$, $g_3 - g_2$, and $g_4 - g_2$, are in column 6 of Table 3. We use these terms to test the consistency of the results. We

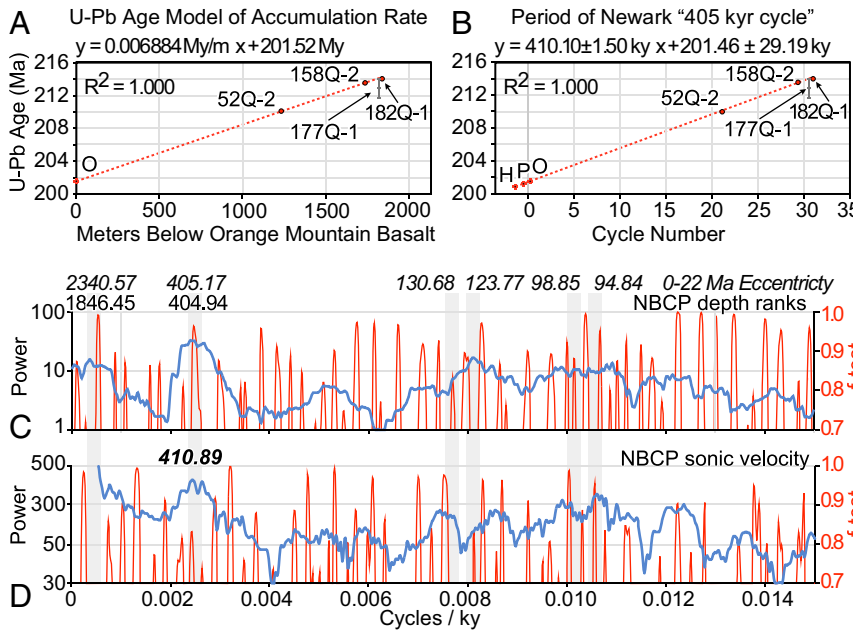


Fig. 4. Simple age model for untuned NBCP data using zircon U-Pb CA-ID-TIMS dates from basalt flows in the Newark Basin section (21) and CPCP-1 dates projected onto the Newark Basin section (12). Vertical gray bars guide the eye to periods from the La2004 solution of 0–22 Ma, with periods shown at the top of C for reference. (A) Accumulation rate determined using the Orange Mt. Basalt date (21) and the CPCP-1 dates with small uncertainties (12) (shown by diameter of point). (B) Duration of Jupiter-Venus Grand Cycle based on counting long (\sim 60-m) filtered cycles from untuned NBCP depth rank data (SI Appendix, Fig. S7 and Table S3); 52Q-1, 185Q-2, and 182Q-1 CPCP-1 dates, and 177Q-1 is the CPCP-1 date with large uncertainty that was not used. H, Hook Mt. Basalt; O, Orange Mt. Basalt; P, Preakness Basalt. (C and D) MTM spectra based on age model in A of untuned sequence of NBCP depth ranks (C) and sonic velocity (D) over the interval with independent dates with a prominent period at \sim 405 ky, periods close to the short eccentricity cycle, and a period close to the Mars-Earth Grand Cycle.

compare the values obtained by FA on the Newark-Hartford data with the corresponding combination of the previously determined values for g_1 through g_4 (with g_5 considered a constant). The differences are very small and are reported in column 5 of Table 3.

The correspondence of the 10 eccentricity terms reported in Table 3 is striking, and it is desirable to quantitatively examine whether such a close fit is due to chance. Among these 10 terms, we will not consider g_5 , because it is assumed constant. Also, we will not consider g_2 , because the Newark-Hartford data are tuned to the $g_2 - g_5$ term. We will not consider $g_4 - g_3$, as we chose the

La2010d* solution, because $g_4 - g_3$ is close to $g_4 - g_3$ of the Newark-Hartford data of Early Mesozoic time. There remain seven frequencies in the Newark-Hartford data that are extremely close to the main La2010d* frequencies. Considering that these seven frequencies are among the 12 terms of largest amplitude of the Newark-Hartford data (after disregarding the $g_2 - g_5$ and $g_4 - g_3$ terms), we performed a statistical experiment with 33 billion draws of 12 frequencies in the [0.20 "/y] interval. The probability that the close match of 7 of 12 terms of the Newark-Hartford to the La2010d* frequencies is due to chance is less than 5×10^{-8}

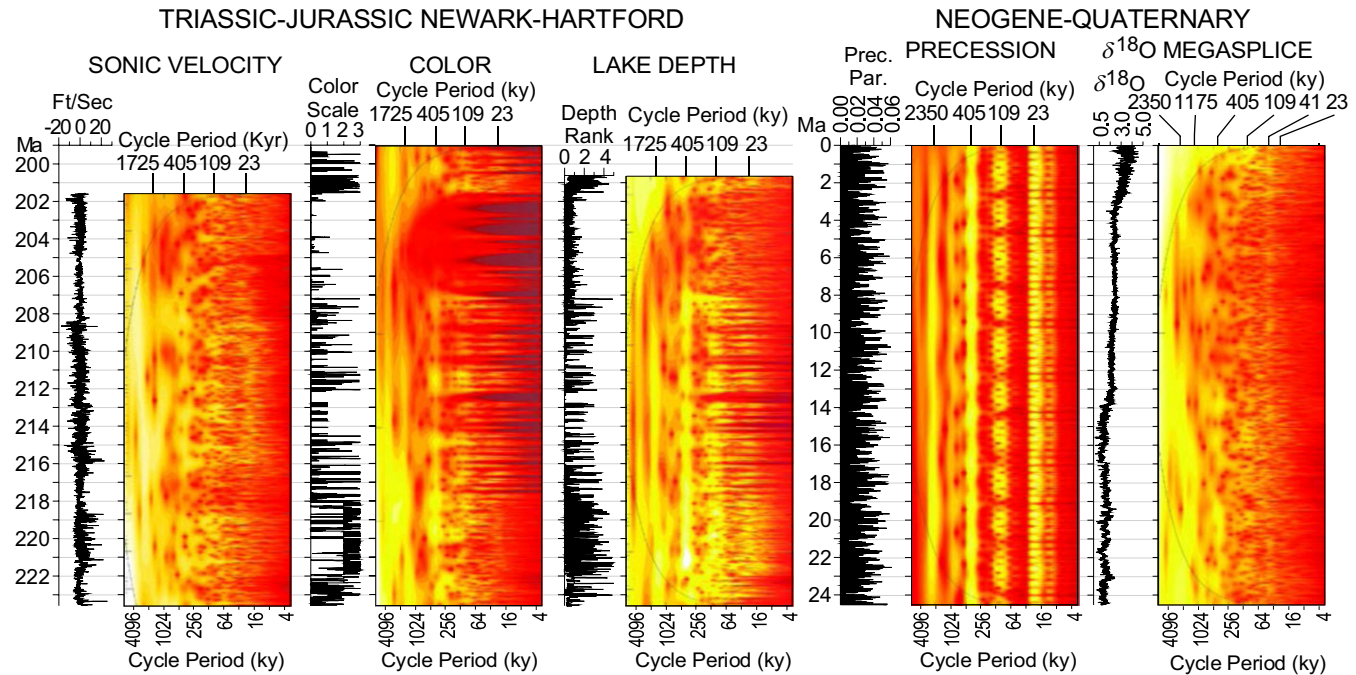


Fig. 5. Comparison of time domain wavelet spectra of similar length from the Newark-Hartford dataset and the last \sim 24 My of the Neogene and Quaternary ($\delta^{18}\text{O}$ Megasplice) (details are in SI Appendix). The Newark-Hartford periods homologous to those in the precession index are apparent as is the difference in the Mars-Earth cycle between the more ancient solution and the modern solution. Note that periodicities at the lower frequencies show up as pulsing in amplitude in the higher frequencies. Precession is derived from clipped precession index of La2004 (29), and the $\delta^{18}\text{O}$ Megasplice is from ref. 49.

Table 3. Secular fundamental frequencies and consistency relations

Row	Argument	MTM ("/y) Newark–Hartford	FA ("/y) Newark–Hartford	FA La2010d* residual ("/y)	La2010d* ("/y)	La2010 ("/y)
0	g5	4.257482 [†]	4.257482 [†]		4.257438	4.257482
1	g4 – g3 [‡]	0.742	0.727 [‡]	0.014 [†]		
2	(g1) [§]	5.662	(5.661) [§]	(0.050) [§]	(5.611) [§]	5.59
3	g2 – g1 [‡]	1.795	1.796 [‡]	0.006 [‡]		
4	(g2 – g5) – (g4 – g3) [‡]	2.456	2.473	-0.016 [‡]		
5	(g2) [§]	7.456	(7.458) [§]	-0.003 [†]	7.461	7.453
6	g3 – g2 [‡]	9.783	9.788 [‡]	0.017 [‡]		
7	g4 – g2 [‡]	10.526	10.516 [‡]	0.014 [‡]		
8	(g3) [§]	17.240	(17.246) [§]	(0.010) [§]	(17.236) [§]	17.368
9	(g4) [§]	17.982	(17.973) [§]	(0.018) [§]	(17.955) [§]	17.916

[†]Assumed values; g5 is considered a constant, and g2 is obtained from g2 – g5 to which the data are tuned.

[‡]The g_i values obtained from the g_i – g5 terms as identified in the Newark–Hartford data.

[§]Consistency check values computed with determined g_i values compared with the Newark–Hartford value from FA.

and on the order of 10⁻¹¹ when only seven frequencies are considered (*SI Appendix*, Figs. S13 and S14). We can thus be very certain that the recovered frequencies in the Newark–Hartford data are actually the secular frequencies of the orbital motion of the Earth, and it is remarkable to see the high precision with which these frequencies are determined (Table 3). While similar values were calculated for the NBCP data in 1999 (22), these values are much more precise and accurate and pass the stringent tests inherent in the relationships among the secular frequencies, their expression in orbital eccentricity cycles, and their independent U–Pb-based age model. It is worth noting that the difference between La2010d* and the Newark–Hartford measurement for the secular fundamental frequency of the precession of perihelion for Mercury of 0.050 "/y (Table 3) is nearly an order of magnitude less than the 0.430 "/y contribution of General Relativity in the precession of perihelion of Mercury (e.g., refs. 2, table 4 and 36).

Other Geologic Expressions of the Mars–Earth (g4 – g3) Cycle in the Newark Basin

The existence of an ~1.75-My cycle in the Triassic age strata of the Newark Basin was first inferred from outcrop data (18), although a 2-My period was estimated at that time. Based on this analysis, that intervals of maximum precessional variability at the peaks of this cycle contain all of the formally named members of the vast Passaic Formation, such as the Perkasie Member, which was originally recognized as distinctive in 1895 (37). These intervals also tend to be the units most easily mapped and the units with the most fossils (9), all of which are evidence of the tangibility of these Grand Cycles (*SI Appendix*, Figs. S15 and S16).

Synthetic seismic traces generated from the borehole data of the NBCP show the Grand Cycles (*SI Appendix*, Fig. S15). When tied to deep industry exploratory borehole records from the Newark Basin, themselves tied to seismic ties, both the Jupiter–Venus 405-ky and Mars–Earth 1.75-My cycles can be clearly seen as the most coherent components of the seismic profiles across the basin (38) (*SI Appendix*, Fig. S15). Presumably due to differences in cementation expressed in sonic parameters, the topographic expression of the deeply eroded tilted strata of the Newark Basin section also reveals the Grand Cycles, which can be seen from space, with ridges reflecting time intervals of high-precessional variability and valleys reflecting low-precessional variability that can be directly tied to the stratigraphy (*SI Appendix*, Fig. S16), much as bundles of plausibly obliquity-related rhythms can be seen in crater walls (39) or polar-layered deposits (40) on Mars.

Comparable Early Mesozoic Results

Thus far, Mesozoic records of astronomical forcing have tended to rely on “floating” astrochronologies or highly tuned records. By designing an experiment in a completely different region, CPCP-1, a globally exportable paleomagnetic and U–Pb-based correlative timescale was produced that validated the NH APTS. In so doing, we show the strong fidelity of the 405-ky Jupiter–Venus cycle as predicted by astronomical solutions, which in turn, allows us to recognize deviations from current astronomical solutions extrapolated from the ~60-Ma limit of reliability, especially for the cycles with periods longer than 405 ky.

Pelagic ribbon-chert sequences from Japan have been correlated to the Newark–Hartford data through mainly biostratigraphic webs and carbon isotope stratigraphy (41). These show remarkably similar periods for the Mars–Earth orbital eccentricity cycle. As with the Newark and Hartford Basins, these were deposited in a tropical environment, albeit in the middle of the Panthalassic Ocean (41). In these data, the most prominent low-frequency cycle has a period that varies between 1.8 and 1.6 My, estimated by counting putative climate precession chert-clay couplets. As with the Newark–Hartford data, there does not seem to be any influence of obliquity.

The Early Jurassic age (Hettangian–Sinemurian) epicontinental marine Bristol Channel Basin (United Kingdom) sequence is precession dominated, expressing eccentricity cycles (42–45), and has a well-developed astrochronology and paleomagnetic polarity stratigraphy that parallels that in the Newark–Hartford composite. Based on polarity stratigraphy correlation to the NH APTS (43), the 405-ky cyclicity is in phase with that in the Newark–Hartford section and shows an amplitude modulation in phase with the g4 – g3 cycle in the radioisotopically anchored Newark–Hartford composite (43, 44). Paleomagnetic polarity correlation between the Newark–Hartford composite to the Bristol Channel section and ammonite-based correlation of the Hettangian–Sinemurian boundary from the Bristol Channel section to the marine Pucara Group (Peru) allows zircon U–Pb ages to be exported to the Bristol Channel and the Newark–Hartford Jurassic sections. The Pucara section has many zircon U–Pb CA-ID-TIMS dated ash layers with ages (46, 47) in agreement with both the Newark–Hartford and Bristol Channel Basin astrochronologies (44). An alternation in intensity of cycles attributed to climatic precession suggests a hint of obliquity pacing in the Bristol Channel data (42, 45) consistent with its higher-latitude position during the Early Jurassic (~32° N) relative to the Newark–Hartford record (~21° N) (10). A similar, stronger indication of obliquity is in results from higher-latitude Rhaetian coal-bearing sequences of the Sichuan Basin in China (48).

Comparison with the Cenozoic and Search for Obliquity Modulation

Comparisons of the recent compilation of benthic foraminifera $\delta^{18}\text{O}$ data “Megasplice” (49) and modulators of obliquity with the astronomical solution for eccentricity and the Newark data are informative (Figs. 5 and 6). The wavelet spectrum of the $\delta^{18}\text{O}$ benthic Megasplice has a less resolved structure than the Newark data. This is also seen in the MTM spectrum. The short orbital eccentricity cycles are well resolved as is the Jupiter–Venus 405-ky cycle; however, all of these cycles were used in tuning the geologically older records that comprise the Megasplice, while geologically younger parts used an age model based on the Lisiecki and Raymo (50) model termed LR04 that incorporated an ice model using the Laskar 1993 solution (La93) (51) for tuning the individual records that make up the LR04 stack; therefore, their agreement with the orbital solutions is not independent (Fig. 6). The obliquity modulating cycles (Fig. 6) are like the eccentricity cycles in that all of the frequencies are combination tones of s_1, s_2, \dots, s_5 , which are related to precession of the node of each planetary orbit (e.g., s_5 is related to the precession of the nodes of the orbit of Jupiter). We can even use the term Grand Cycles of obliquity to refer to the ensemble of long-period cycles.

The MTM spectrum of obliquity shows what should be expected in the Newark or $\delta^{18}\text{O}$ benthic Megasplice if obliquity was a major component of the records. There is no obvious signal that can be assigned to combinations of the Grand Cycle s_1, s_2, \dots, s_5 secular frequencies in the Newark–Hartford data, although there could be confusion between the obliquity cycles around 100 ky and the short eccentricity cycles. Surprisingly, however, there is also no clear obliquity signal in the MTM spectrum of the $\delta^{18}\text{O}$ benthic Megasplice as represented here either, although some beats, especially the 1.2-My ($s_4 - s_3$) Grand Cycle, are evident in the wavelet spectrum, and they have been reported from the older components of the $\delta^{18}\text{O}$ benthic Megasplice, not examined here, and used to constrain astronomical solutions (52). Based on the wavelet spectrum, the obliquity Grand Cycles are smeared out in the younger part of the Megasplice record. This is despite the fact that obliquity and its longer-period modulators are known to be a significant part of the pacing of climate as seen in some of the records making up the Megasplice and high-latitude non-marine records (52–54). Whether this reflects real aspects of

the climate system, perhaps damped by low CO₂; mixing of signals from different parts of the climate system; the $\delta^{18}\text{O}$ proxy itself; or issues with tuning requires much additional work.

Grand Cycles and the Roadmap to Solar System Chaos

The results from the wavelet, MTM spectra, and FA of the Newark–Hartford data (Figs. 5 and 6 and Tables 2 and 3) are remarkable, because while the calculations of the Grand Cycles from the short eccentricity cycles in the 0- to 22-Ma data are due to their necessary linkage in the way that the astronomical solution is deconvolved and the secular frequencies are resolved, the succession of rock layers 210 My old has no such necessary linkage; it can only result from the sedimentary record of the climate response to the same physics that are imbedded in the 0- to 22-Ma eccentricity solution playing out in time. The differences between the current g_1 through g_4 values (column 7 of Table 3) and their Newark–Hartford FA determinations (column 4 of Table 3) are, therefore, significative and most parsimoniously explained as the result of chaotic diffusion in the gravitational interactions of the Solar System. In particular, the drift of $g_4 - g_3$ from the 2.36-My present value to the 1.75-My period observed in the Newark–Hartford data can be considered as direct geological evidence of the chaotic behavior of the Solar System.

Strong evidence for Grand Cycle orbital eccentricity pacing of climate is widespread in the lower latitudes during the Late Triassic and Early Jurassic. However, the results presented here suggest that the present astronomical solution for eccentricity does not fit the frequency data well for this time period (Table 3). We found a good match with the La2010d* solution, but it is expected that a more systematic search of the possible variations of the astronomical solutions could lead to an even better match. The important result for the Newark–Hartford data is to provide precise values for the Triassic–Jurassic secular fundamental frequencies g_1 through g_4 that could be considered as a reference point and used as an anchor for the search of orbital solutions that could match the past orbital evolution of the Solar System as recorded in the sedimentary data.

However, a major contributor to the chaotic behavior, in fact its signature (30), is related to the Mars–Earth secular resonance ($g_4 - g_3$) – $2(s_4 - s_3)$ (now in libration; i.e., oscillation in phase space) and its possible transitions to and from ($g_4 - g_3$) – ($s_4 - s_3$) (circulation; i.e., rotation in phase space), with the resulting 2:1 vs.

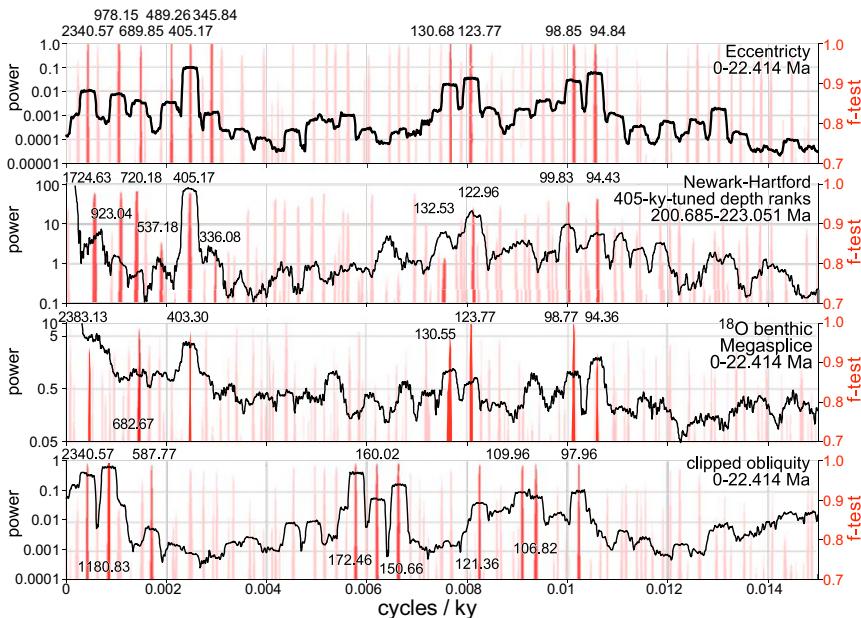


Fig. 6. MTM spectra from the La2004 solution for eccentricity (29), 405-ky tuned Newark–Hartford depth rank data, the $\delta^{18}\text{O}$ benthic Megasplice (50), and clipped La2004 solution for obliquity (33) (Analyses 2.0 default: 6, 4 pi tapers). A 0- to 22-Ma interval instead of 0–24 Ma (as in the color data in Fig. 3) was used to conform to the depth rank data as opposed to the 0- to 24-Ma color data (Fig. 3). Periods above each spectrum are labeled where there is both high power and a high f significance level. Newark–Hartford data are tuned only to the 405-ky Jupiter–Venus cycle ($g_2 - g_5$), while the $\delta^{18}\text{O}$ benthic Megasplice (50) is a composite of several records individually tuned to a suite of periodicities, including all of the major eccentricity periods from 405 to ~100 ky for the older records and obliquity and the LR03 stack for the younger ones (50) (SI Appendix).

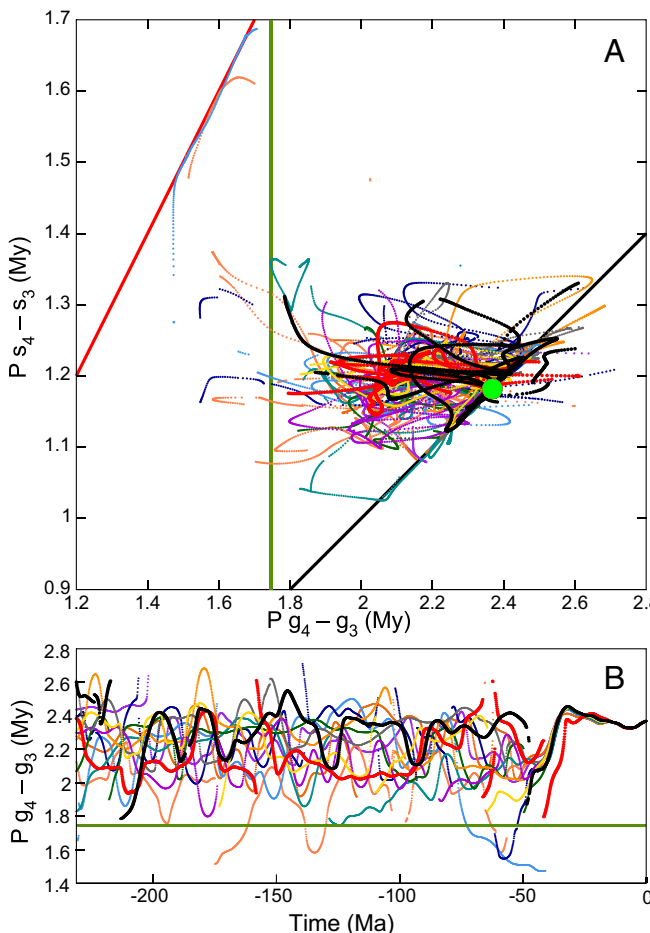


Fig. 7. Evolution of the period (P) of the $g_4 - g_3$ and $s_4 - s_3$ terms in 13 numerical solutions of the Solar System integrated over 250 My in the past. Frequencies values are obtained by FA over a sliding interval of 20 My, with an offset of 1 My between each interval. (A) The period of $s_4 - s_3$ is plotted with respect to the $g_4 - g_3$ period. The diagonal black line corresponds to the 2:1 resonance [$P(g_4 - g_3) = 2P(s_4 - s_3)$], where P stands for “period of”, while the red line is the 1:1 resonance [$P(g_4 - g_3) = P(s_4 - s_3)$]. The green circle at (2.4, 1.2) is the present value for the Solar System and starting point of all solutions. (B) $P(g_4 - g_3)$ is plotted for all 13 solutions. The black curve corresponds to La2010d (5), and the red curve is the La2004 (29). In both A and B, the green line is $P(g_4 - g_3) = 1.75$ My, the observed Newark-Hartford value.

1:1 periods of the eccentricity and obliquity Grand Cycles (Fig. 7A). Because the Newark–Hartford data show no clearly discernible obliquity pacing, the mode of 2:1 vs. 1:1 resonance in the secular frequencies cannot presently be determined for this time interval. While there has been some recent progress with tantalizing results (55), the transition from the 2:1 vs. 1:1 periods has yet to be unambiguously observed in suitably long records, and it is possible that it has never occurred, although most numerical solutions show it. To obtain a result for the Triassic–Jurassic secular resonance, suitably long (>10-My) contemporaneous high-latitude records that would be expected to show a strong obliquity pacing are needed. For example, the continental and coal-bearing Triassic–Jurassic ~70° N Junggar Basin section shows strong hints of obliquity forcing interpreted to be a 2:1 ratio of eccentricity to obliquity Grand Cycles (~1.6:0.8 Ma), but that section lacks an independent geochronologic or paleomagnetic polarity timescale, although it does exhibit 405-ky periodicity (44). Cores spanning tens of millions of years from such a section would permit a high-resolution paleomagnetic polarity record to be developed from the basin (extremely difficult to do in outcrop in these gray and black strata

because of weathering) that would allow correlation to the Newark–Hartford data and presumably resolve the mode of resonance in the eccentricity and obliquity Grand Cycles. This would be a full proof of concept of the Geological Orrery.

If the resonance is in the 2:1 ratio for the latest Triassic and earliest Jurassic as the preliminary interpretations suggest, this finding would only apply to that particular time, and we still cannot show when or if the 1:1 situation ever happens. There are strong hints that even longer astronomical cycles with periods of ~8–9 and ~36 My (41, 56) may modulate the Grand Cycles, and these modulations could be confused with actual changes in secular frequencies or tectonic influences in records that are too short. To examine these potential empirical phenomena will require careful concatenation of multiple long records with appropriate properties, including independent geochronology, all accurately recording low and high frequencies that pass the types of rigorous tests outlined here.

A complete Geological Orrery would consist of multiple sets of paired low- and high-latitude records (preferably cored to ensure superposition and continuity) spanning the Paleogene to Permian and beyond, with even deeper time highly desirable. When combined with the existing record from the last ~60 My, the last ~250 My of Solar System history would be covered. The empirical mapping of the secular frequencies of the Grand Cycles in eccentricity and obliquity over this time interval (including the transitions in secular resonances should they occur) would constitute an entirely new empirical realm to test Solar System evolution, astronomical solutions, and gravitational models. By constraining the past evolution of the speed of perihelion of Mercury g_1 , the results would provide mechanisms to constrain the evolution of the flattening parameter J_2 of the Sun and further test General Relativity and its alternatives (3). The constraint on the past evolution of the other secular frequencies may be used to limit the existence of additional planets and examine predictions of galactic disk dark matter interactions with the Solar System (56, 57). The results would also be important in efforts to tune radiometric decay constants for geochronology and to produce accurate solar insolation targets beyond 60 Ma.

Materials and Methods

Core used in this analysis originates from three sedimentary basins in North America (SI Appendix, Fig. S1): the cores from the seven NBCP core sites (Newark Basin), the Passaic River Diversionary Tunnel Army Corps of Engineers (ACE) cores (Newark Basin), the Silver Ridge Core (Hartford Basin), the Park River Cores (Hartford Basin), the Metropolitan District Commission (MDC) cores (Hartford Basin), and the Colorado Plateau Coring Project, Petrified Forest National Park, 2013 1A (CPCP-PFPN13-1A) core (Colorado Plateau). Details of locations are given in SI Appendix, Table S1.

MTM spectra (Figs. 3, 4, and 6 and SI Appendix, Fig. S9) were developed using Analyseries (2.0), which was also used for filtering, interpolation, etc. (58), and the wavelet spectra (Figs. 2, 3, and 5 and SI Appendix, Figs. S6 and S12) were computed using the Matlab script of Torrence and Compo (59) (paos.colorado.edu/research/wavelets). For all data, Analyseries (2.0) was used for interpolation and for the time series based on the Laskar 2004 solution (29), which in the case of the last 0–24 Ma, is not significantly different from more recent solutions (5). The FA method is described in refs. 30 and 31 and has been used with its implementation in the TRIP software, which is documented and freely available at <https://www.imcce.fr/trip/>. The TRIP source code used in this work is given in SI Appendix. Work on the NBCP and CPCP-1 cores was conducted at the Rutgers Core Repository as described in ref. 12, and CPCP-1 core analysis and documentation were conducted at the LacCore facility at the University of Minnesota (11).

ACKNOWLEDGMENTS. We are grateful for the encouragement and guidance of NSF program directors Leonard Johnson and the late Richard Lane leading up to and during the funded phases of the NBCP and the CPCP, respectively. We thank Randy Steinen for access to the Metropolitan District Commission Hartford Basin cores and Margaret Thomas and Randy Steinen for access to the Park River cores. We thank Clara Chang for help with Itrax X-ray fluorescence data collection and processing as well as proofing. We also thank the National Park Service, particularly superintendent Brad Traver for permission to core and William Parker for encouragement and advice during coring and the predrilling workshops. Curatorial facilities for the work halves of the CPCP-1 cores and all of the NBCP and ACE cores are provided by the Rutgers Core Repository, and we thank James Browning for access. This

project was funded by NSF Grant EAR 8916726 (to P.E.O. and D.V.K.) for the NBCP and the CPCP, Collaborative Grants EAR 0958976 (to P.E.O.) and 0958859 (to D.V.K.), and International Scientific Continental Drilling Program Grant 05-2010. P.E.O. and S.T.K. acknowledge support from the Lamont Climate Center, and P.E.O. completed this paper while on sabbatical as a visiting scientist at Amherst College's Beneski Museum. J.L. acknowledges support from the Programme National de Planéologie and the Paris Observatory Scientific Council. D.V.K. acknowledges the Lamont-Doherty Incentive Account for support of the Paleomagnetics Laboratory. S.T.K. ac-

knowledges support from NSF Graduate Research Fellowship Program Grant DGE 16-44869. J.H.W. recognizes support from an Annual Adventures in Research Award from University of Southampton and NSF EAR 1349650. This work was partly supported by National Natural Science Foundation of China Grant 41730317, Special Basic Program of Ministry of Science and Technology of China Grant 2015FY310100, the Bureau of Geological Survey of China, and National Committee of Stratigraphy of China Grant DD20160120-04. This is a contribution to International Geological Correlation Program-632, and it is Lamont-Doherty Earth Observatory Contribution 8285.

1. Laplace PS Marquis de (1812) *Théorie Analytique des Probabilités* (Courcier, Paris).
2. Laskar J (1999) The limits of Earth orbital calculations for geological time-scale use. *Phil Trans Roy Soc Lond A* 357:1735–1759.
3. Laskar J (2003) Chaos in the solar system. *Ann Henri Poincaré* 4:693–705.
4. Pálike H, Laskar J, Shackleton N (2004) Geologic constraints on the chaotic diffusion of the solar system. *Geology* 32:929–932.
5. Laskar J, Fienga A, Gastineau M, Manche H (2011) La2010: A new orbital solution for the long-term motion of the Earth. *Astron Astrophys* 532:L1–15.
6. Buick T (2013) *Orrery: A Story of Mechanical Solar Systems, Clocks, and English Nobility* (Springer, New York).
7. Applegate JH, et al. (1986) A digital orrery. *The Use of Supercomputers in Stellar Dynamics*, eds Hut P, McMillan SL (Springer, Berlin), pp 86–95.
8. Sussman GJ, Wisdom J (1992) Chaotic evolution of the solar system. *Science* 257:56–62.
9. Olsen PE, Kent DV, Cornet B, Witte WK, Schlysche RW (1996) High-resolution stratigraphy of the Newark rift basin (early Mesozoic, eastern North America). *Geol Soc Am Bull* 108:40–77.
10. Kent DV, Olsen PE, Muttoni G (2017) Astrochronostigraphic polarity time scale (APTS) for the Late Triassic and Early Jurassic from continental sediments and correlation with standard marine stages. *Earth Sci Rev* 166:153–180.
11. Olsen PE, et al. (2018) Colorado plateau coring project, phase I (CPCP-I): A continuously cored, globally exportable chronology of Triassic continental environmental change from Western North America. *Sci Drill* 24:15–40.
12. Kent DV, et al. (2018) Empirical evidence for stability of the 405 kyr Jupiter-Venus eccentricity cycle over hundreds of millions of years. *Proc Natl Acad Sci USA* 115:6153–6158.
13. Olsen PE, Schlysche RW, Fedosch MS (1996) 580 kyr duration of the Early Jurassic flood basalt event in eastern North America estimated using Milankovitch cyclostratigraphy. *The Continental Jurassic*, Museum of Northern Arizona Bulletin 60, ed Morales M, (Museum of Northern Arizona, Flagstaff, AZ), pp 11–22.
14. Whiteside JH, Olsen PE, Kent DV, Fowell SJ, Et-Touhami M (2007) Synchrony between the CAMP and the Triassic-Jurassic mass-extinction event? *Palaeogeogr Palaeoclimatol Palaeoecol* 244:345–367.
15. Kent DV, Olsen PE (2008) Early Jurassic magnetostratigraphy and paleolatitudes from the Hartford continental rift basin (eastern North America): Testing for polarity bias and abrupt polar wander in association with the Central Atlantic Magmatic Province. *J Geophys Res* 113:B06105.
16. Kent DV, Tauxe L (2005) Corrected Late Triassic latitudes for continents adjacent to the North Atlantic. *Science* 307:240–244.
17. Van Houten FB (1964) Cyclic lacustrine sedimentation, Upper Triassic Lockatong Formation, central New Jersey and adjacent Pennsylvania. *Symposium on Cyclic Sedimentation*, Kansas Geological Survey Bulletin 169, ed Mermiam OF, (Kansas Geological Survey, Lawrence, KS), pp 497–531.
18. Olsen PE (1986) A 40-million-year lake record of early mesozoic orbital climatic forcing. *Science* 234:842–848.
19. Olsen PE, Kent DV (1996) Milankovitch climate forcing in the tropics of Pangea during the Late Triassic. *Palaeogeogr Palaeoclimatol Palaeoecol* 122:1–26.
20. Kent DV, Olsen PE, Witte WK (1995) Late Triassic-earliest Jurassic geomagnetic polarity sequence and paleolatitudes from drill cores in the Newark rift basin, eastern North America. *J Geophys Res* 100:14965–14998.
21. Blackburn TJ, et al. (2013) Zircon U-Pb geochronology links the end-Triassic extinction with the Central Atlantic Magmatic Province. *Science* 340:941–945.
22. Olsen PE, Kent DV (1999) Long-period Milankovitch cycles from the Late Triassic and Early Jurassic of eastern North America and their implications for the calibration of the Early Mesozoic time-scale and the long-term behaviour of the planets. *Philos Trans R Soc Lond A* 357:1761–1786.
23. Olsen PE (2001) Grand cycles of the Milankovitch band. *Eos Tran Amer Geophys Union* 82:F2 (abstr U11A-11).
24. Hilgen FJ, Krijgsman W, Langereis CG, Lourens LJ (1997) Breakthrough made in dating of the geological record. *Eos (Wash DC)* 78:285–289.
25. Tanner LH, Lucas SG (2015) The Triassic-Jurassic strata of the Newark Basin, USA: A complete and accurate astronomically-tuned timescale? *Stratigraphy* 12:47–65.
26. Van Veen PM (1995) Time calibration of Triassic/Jurassic microfloral turnover, eastern North America—comment. *Tectonophysics* 245:93–95.
27. Kozur H, Weems RE (2005) Conchostracean evidence for a late Rhaetian to early Hettangian age for the CAMP volcanic event in the Newark Supergroup, and a Sevonian (late Norian) age from the immediately underlying beds. *Hallesches Jahrb Geowiss* B27:21–51.
28. Laskar J (2003) Frequency map analysis and particle accelerators. *Proceedings of the 2003 Particle Accelerator Conference*, eds Chew J, Lucas P, Webber S (IEEE, Portland, OR), Vol 1, pp 378–382.
29. Laskar J, et al. (2004) A long-term numerical solution for the insolation quantities of the Earth. *Astron Astrophys* 428:261–285.
30. Laskar J (1990) The chaotic motion of the solar system: A numerical estimate of the size of the chaotic zones. *Icarus* 88:266–291.
31. Laskar J (2005) Frequency map analysis and quasi periodic decompositions. *Hamiltonian Systems and Fourier Analysis: New Prospects for Gravitational Dynamics*, *Advances in Astronomy*, eds Benest D, Froeschle C, Lega E (Taylor and Francis, Cambridge, United Kingdom), pp 99–130.
32. Robin D, Steier C, Laskar J, Nadolski L (2000) Global dynamics of the advanced light source revealed through experimental frequency map analysis. *Phys Rev Lett* 85:558–561.
33. Berger A, Loutre MF, Laskar J (1992) Stability of the astronomical frequencies over the Earth's history for paleoclimate studies. *Science* 255:560–566.
34. Berger A, Loutre MF (1990) Origine des fréquences des éléments astronomiques intervenants dans le calcul de l'insolation. *Bull Class Sci Acad Roy Belg Ser 6* 1:45–106.
35. Laskar J, Gastineau M, Delisle J-B, Farres A, Fienga A (2011) Strong chaos induced by close encounters with Ceres and Vesta. *Astron Astrophys* 532:L4.
36. Will CM (2006) The confrontation between general relativity and experiment. *Living Rev Relativ* 9:3.
37. Lyman BS (1895) *New Red of Bucks and Montgomery Counties, [Pennsylvania]. Final Report Ordered by Legislature, 1891; a Summary Description of the Geology of Pennsylvania* (Pennsylvania Geological Survey, Harrisburg, PA), Vol 3, pp 2589–2638.
38. Reynolds DJ (1993) Sedimentary basin evolution: Tectonic and climatic interaction. PhD thesis (Columbia University, New York).
39. Lewis KW, et al. (2008) Quasi-periodic bedding in the sedimentary rock record of Mars. *Science* 322:1532–1535.
40. Laskar J, Levrad B, Mustard JF (2002) Orbital forcing of the martian polar layered deposits. *Nature* 419:375–377.
41. Ikeda M, Tada R (2013) Long period astronomical cycles from the Triassic to Jurassic bedded chert sequence (Inuyama, Japan); Geologic evidences for the chaotic behavior of solar planets. *Earth Planets Space* 65:351–360.
42. Ruhl M, et al. (2010) Astronomical constraints on the duration of the early Jurassic Hettangian stage and recovery rates following the end-Triassic mass extinction (St. Audrie's Bay/East Quantoxhead, United Kingdom). *Earth Planet Sci Lett* 295:262–276.
43. Hüsing SK, et al. (2014) Astronomically-calibrated magnetostratigraphy of the Lower Jurassic marine successions at St. Audrie's Bay and East Quantoxhead (Hettangian-Sinemurian; Somerset, UK). *Palaeogeogr Palaeoclimatol Palaeoecol* 403:43–56.
44. Sha J, et al. (2015) Early Mesozoic, high-latitude continental Triassic-Jurassic climate in high-latitude Asia was dominated by obliquity-paced variations (Junggar Basin, Urumqi, China). *Proc Natl Acad Sci USA* 112:3624–3629.
45. Xu W, Ruhl M, Hesselbo SP, Riding JB, Jenkyns HC (2017) Orbital pacing of the Early Jurassic carbon cycle, black-shale formation and seabed methane seepage. *Sedimentology* 64:127–149.
46. Guex J, et al. (2012) Geochronological constraints on post-extinction recovery of the ammonoids and carbon cycle perturbations during the Early Jurassic. *Palaeogeogr Palaeoclimatol Palaeoecol* 346:1–11.
47. Yager JA, et al. (2017) Duration of and decoupling between carbon isotope excursions during the end-Triassic mass extinction and Central Atlantic Magmatic Province emplacement. *Earth Planet Sci Lett* 473:227–236.
48. Li M, et al. (2017) Astronomical tuning and magnetostratigraphy of the Upper Triassic Xujiahe formation of South China and Newark supergroup of North America: Implications for the late Triassic time scale. *Earth Planet Sci Lett* 475:207–223.
49. De Vleeschouwer D, Vahlenkamp M, Crucifix M, Pálike H (2017) Alternating Southern and Northern Hemisphere climate response to astronomical forcing during the past 35 m.y. *Geology* 45:375–378.
50. Lisiecki LE, Raymo ME (2005) A Pliocene-Pleistocene stack of 57 globally distributed benthic $\delta^{18}\text{O}$ records. *Paleoceanography* 20:PA1003.
51. Laskar JF, Joutel F, Boudin F (1993) Orbital, precessional and insolation quantities for the Earth from -20 Myr to +10 Myr. *Astron Astrophys* 270:522–533.
52. Pálike H, et al. (2006) The heartbeat of the Oligocene climate system. *Science* 314: 1894–1898.
53. van Dam JA, et al. (2006) Long-period astronomical forcing of mammal turnover. *Nature* 443:687–691.
54. Prokopenko AA, et al. (2006) Orbital forcing of continental climate during the Pleistocene: A complete astronomically tuned climatic record from Lake Baikal, SE Siberia. *Quat Sci Rev* 25:3431–3457.
55. Ma C, Meyers SR, Sageman BB (2017) Theory of chaotic orbital variations confirmed by Cretaceous geological evidence. *Nature* 542:468–470.
56. Bouilila S, et al. (2018) Long-term cyclicity in Phanerozoic sea-level sedimentary record and their potential drivers. *Global Planet Change* 165:128–136.
57. Rampino MR (2015) Disc dark matter in the Galaxy and potential cycles of extraterrestrial impacts, mass extinctions and geological events. *Monthly Notices roy. Astron Soc* 448:1816–1820.
58. Paillard D, Labeyrie L, Yiou P (1996) Macintosh program performs time-series analysis. *Eos (Wash DC)* 77:379.
59. Torrence C, Compo GP (1998) A practical guide to wavelet analysis. *Bull Am Meteorol Soc* 79:61–78.
60. Ramsey M (2018) Schlumberger oilfield glossary. Available at https://www.glossary.oilfield.slb.com/en/terms/r/reflection_coefficient.aspx. Accessed February 13, 2019.



Supplementary Information for
Mapping Solar System Chaos with the Geological Orrery

P.E. Olsen, J. Laskar, D.V. Kent, S.T. Kinney, D.J. Reynolds, J. Sha, and J.H. Whiteside

Paste corresponding author name here
Email: polsen@ldeo.columbia.edu

This PDF file includes:

Supplementary text
Figs. S1 to S16
Tables S1 to S7
Captions for datasets S1 to S9
References for SI reference citations

Other supplementary materials for this manuscript include the following:

Datasets S1 to S9

Supplementary Information Text

Materials: Cores and Outcrops

Core and outcrops used in this analysis originate from three sedimentary basins in North America (**Fig. S1; Table S1**). Derived from these basins are the following archives: Seven Newark Basin Coring Project (NBCP) cores from seven sites (Newark Basin); the ACE cores (Newark Basin); the Silver Ridge Core (Hartford Basin); the Park River cores (Hartford Basin); the MDC cores (Hartford Basin), outcrops in the Hartford Basin (from ref. 1) and the CPCP-PFNP-13-1A core (Colorado Plateau) (3).

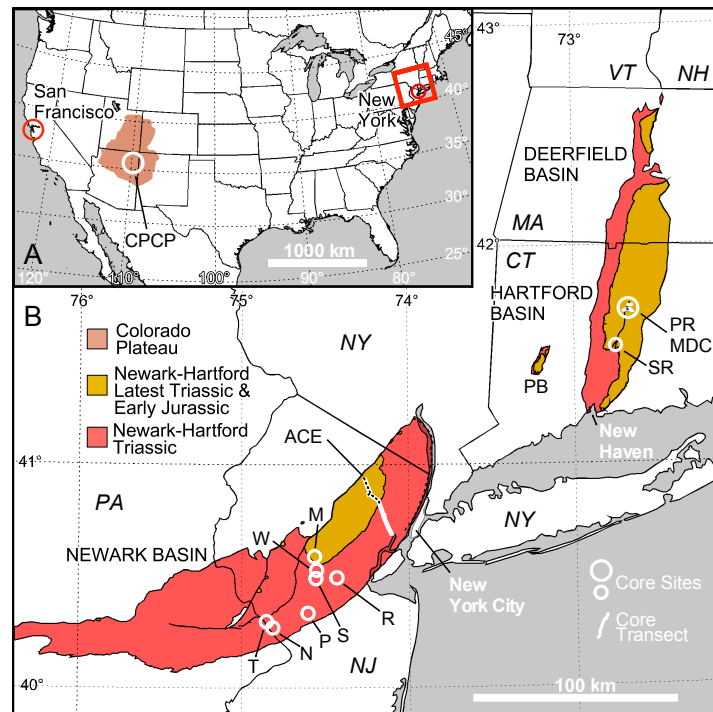


Fig. S1. A, Map of the conterminous United States showing location of the Colorado Plateau, the CPCP coring sites (**Table S1**) and the location (red box) of the Newark and Hartford basin shown in B. B, Map of the Newark and Hartford basins showing positions of core sites used in this study (**Table S1**). Abbreviations are: ACE, Army Corps of Engineers, Passaic River Diversion Tunnel Cores (transect shown as white line with used cores as dotted black line); CPCP, Colorado Plateau Coring Project core sites; M, Martinsville no. 1; MDC, Metropolitan District (Army Corps of Engineers) cores (transect shown as white line with cores used at black dot); N, Nursery no. 1; P, Princeton no. 1 & 2; PB, Pomperaug Basin; PR, Park River (Army Corps of Engineers) cores (described in ref.1); R, Rutgers no. 1 & 2; S, Somerset no. 1 & 2; SR, Silver Ridge B-1 core; Y, Titusville no. 1 & 2; W, Weston Canal no. 1 & 2.

Table S1. Latitude and longitude for cores, coreholes, and outcrops.

Fig. S1	Core / Key Outcrop	Location (decimal deg) ^a Lat (N) Long (W)		Reference	Repository
ACE	C-92	40.885198	74.220787	8	Rutgers-CR ^b
ACE	C-93	40.885151	74.222775	herein	Rutgers-CR ^b
ACE	C-103	40.918175	74.254818	8	Rutgers-CR ^b
ACE	DH-9	40.878893	74.229606	herein	Rutgers-CR ^b
ACE	PT-5	40.951110	74.269873	8	Rutgers-CR ^b
ACE	PT-7	40.943900	74.267700	8	Rutgers-CR ^b

ACE	PT-8	40.939689	74.264427	8	Rutgers-CR ^b
ACE	PT-9	40.935100	74.261400	8	Rutgers-CR ^b
ACE	PT-10	40.928900	74.258600	8	Rutgers-CR ^b
ACE	PT-11	40.927300	74.255700	8	Rutgers-CR ^b
ACE	PT-12	40.924098	74.255754	8	Rutgers-CR ^b
ACE	PT-14	40.916200	74.252700	8	Rutgers-CR ^b
ACE	PT-15	40.911906	74.249639	8	Rutgers-CR ^b
ACE	PT-16	40.908200	74.248998	8	Rutgers-CR ^b
ACE	PT-17	40.903600	74.247100	8	Rutgers-CR ^b
ACE	PT-26	40.878400	74.223600	2	Rutgers-CR ^b
ACE	PT1-B3	40.883900	74.231900	herein	Rutgers-CR ^b
CPCP	CPCP-PFNP13-1A	35.085933	109.795500	3	Rutgers/LacCore ^c
M	Martinsville no. 1	40.611446	74.574368	4	Rutgers-CR ^b
MDC	BD 255	41.737171	72.693138	5	MDC-CF ^f
MDC	BD 226	41.737089	72.695639	5	MDC-CF ^f
MDC	BD 227A	41.737010	72.697214	5	MDC-CF ^f
N	Nursery 1	40.289598	74.823748	4	Rutgers-CR ^b
P	Princeton nos. 1, 2	40.361275	74.613286	4	Rutgers-CR ^b
PR	Park River Core FD-5T	41.757387	72.671077	6	CTGS-RPSCR ^d
PR	Park River Core FD-6T	41.757892	72.669393	6	CTGS-RPSCR ^d
PR	Park River Core FD-12T	41.757841	72.675222	6	CTGS-RPSCR ^d
PR	Park River Core FD-14T	41.758201	72.690903	6	CTGS-RPSCR ^d
PR	Park River Core FD-15T	41.757799	72.678361	6	CTGS-RPSCR ^d
PR	Park River Core FD-16T	41.757913	72.684209	6	CTGS-RPSCR ^d
PR	Park River Core FD-18T	41.758023	72.682255	6	CTGS-RPSCR ^d
PR	Park River Core FD-19T	41.757686	72.672524	6	CTGS-RPSCR ^d
PR	Park River Core FD-20T	41.757929	72.688150	6	CTGS-RPSCR ^d
PR	Park River Core FD-23T	41.757715	72.671683	6	CTGS-RPSCR ^d
PR	Park River Core FD-27T	41.757519	72.663522	6	CTGS-RPSCR ^d
PR	Park River Core FD-28T	41.757536	72.664301	6	CTGS-RPSCR ^d
PR	Park River Core FD-29T	41.757496	72.664766	6	CTGS-RPSCR ^d
PR	Park River Core FD-30T	41.757341	72.668001	6	CTGS-RPSCR ^d
PR	Park River Core FD-31T	41.757573	72.665772	6	CTGS-RPSCR ^d
R	Rutgers nos. 1, 2	40.526411	74.433083	4	Rutgers-CR ^b
S	Somerset nos. 1, 2	40.505764	74.565386	4	Rutgers-CR ^b
SR	Silver Ridge B-1	41.585000	72.756500	7	LDEO ^e
T	Titusville nos. 1, 2	40.318858	74.849922	4	Rutgers-CR ^b
W	Weston Canal nos. 1, 2	40.542116	74.562873	4	Rutgers-CR ^b
outcrop	Watchung Reservation	40.683279	74.380152	2	Watchung Res. ^g

Table S1 Notes

- ^a Google Earth Coordinates (Map Datum WGS84)
- ^b Rutgers Core Repository (<https://geology.rutgers.edu/centers-institutes/rutgers-core-repository>)
- ^c Core split with working half at the Rutgers Core Repository (above) and the archive half at the LacCore Core Facility (<http://lrc.geo.umn.edu/laccore/>)
- ^d DEEP Connecticut Geological Survey, Randolph P. Steinen, Core Repository (http://www.ct.gov/deep/cwp/view.asp?a=2701&q=467634&depNav_GID=1641)
- ^e Lamont-Doherty Earth Observatory of Columbia University
- ^f Metropolitan District Commission Core Facility, Brainard Road (Metropolitan District Commission Core Facility, Brainard Road (<https://themdc.org/>)
- ^g <http://ucnj.org/parks-recreation/trails-greenways/watchung-reservation/>

Newark-Hartford Data

NBCP cores were composited following the procedures in ref. (2) and completely redone, because there were a number of small errors in the original compilation. In brief, in instances where there is a core 1 and 2 at a single site, 1 the data were concatenated using lithology as the primary tool

for correlation. Where there was no clear lithological marker the gamma and sonic logs were used to correlate the two holes, as with Martinsville and Weston Canal. The cores were then stretched and registered to the holes by matching core hole and core gamma (provided by drilling operator AMOCO) peaks except in the case of Weston for which there is no core gamma (drilled by Longyear Inc.). Each core record was scaled to Rutgers using the factors described in (2).

The original composite depth series for the Newark-Hartford cores was interpolated in the recorded drilling units (decimal feet) with an increment of 0.4 ft (0.123 m), except for what is represented in **Fig. 3** where 0.5 ft was used. This was to avoid additional roundoff errors. Results are generally presented in meters or both meters and feet.

Compositing the NBCP geophysical logs. The composite gamma and sonic logs have been assembled from seven down-hole logs using the same scaling factors as above (2). For natural gamma ray data, the compositing was fairly straightforward because there was no major down hole trends. However, the overlapping intervals of adjacent cores had to be scaled to each other in amplitude (**Fig. S2**). Compositing the sonic velocity data was not as straightforward. As can be seen in **Fig. S2**, there are strong trends related to the surface, and each trend requires a different type of detrending that introduced additional degrees of freedom. The detrending was done only on the data below the patch on each successive log (**Fig. S2**). Unfortunately, a residuum of low frequency artifacts cannot be removed and reduces the integrity of the data.

In the Martinsville core, the presence of fracturing around a small fault (probably strike slip) at 2348 feet in log units made a small correction necessary in the sonic velocity data. First a notch filter was used to remove the lowest frequency component corresponding to the fault. The interval 2228-2468 ft was detrended using a sixth order polynomial fit. ($Y = -1.06017426E^{-11} * X^6 + 1.4915498347E^{-7} * X^5 - 8.74059596210677E^{-4} * X^4 + 2.73084509212887 * X^3 - 4797.66288535135 * X^2 + 4493817.46968625 * X - 1753252476.23519$). The Martinsville corrected sonic log was then linearly detrended. For Weston Canal the sonic log was detrended using logarithmic regression using $3.32698017859222 * \ln X + 91.978239908426$. The other borehole logs were detrended linearly.

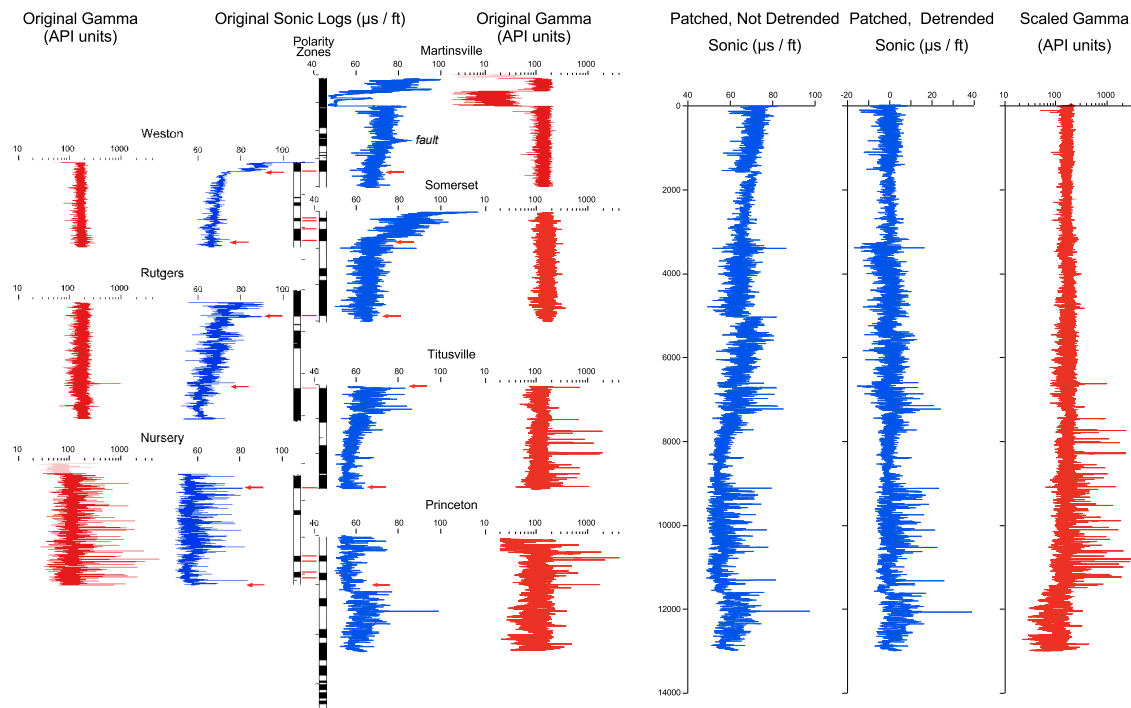


Fig. S2. Composite sonic velocity and natural gamma borehole logs from the NBCP. Red arrows indicate the tie points.

Ace Composite. Towaco and Boonton: Compilation of Towaco (PT-17, PT-16, PT-15, PT-14, C-103, PT-12, PT-11) and Boonton (PT-10, PT-9, PT-8, PT-7, PT-5) cores was straightforward because they are all drilled close together along the Passaic River Tunnel, they have a pronounced cyclicity, and there is substantial stratigraphic overlap and in several cases nearly complete overlap (e.g., C-128, PT-14). This complication is as described in ref. (8). Note that PT-5 is erroneously recorded, as PT-6 in ref. (8); PT-5 does not exist.

Feltville Formation Compilation: ACE cores of the Feltville Formation (PT-26, C-93, DH-9, PT-1B3) were not as straightforward to compile because several were legacy cores, not drilled on the tunnel transect with only one being used (i.e., DH-9). In general, the core holes tended to be considerably shallower, and the upper three quarters of the formation lacks definitely distinctive lacustrine units, complicating correlation. Although the NBCP core Martinsville no. 1, spanned the entire formation the lower part of the Feltville Formation is clearly condensed relative to the ACE cores, distinctly redder, and not representative of the formation (Fig. S3). Hence the cores were linked with the most distinctive beds, and all were compiled with the same depth scale, the upper (~24 m, 80 ft) of the Martinsville no. 1 being used to complete the section (Fig. S3). That the use of the ACE cores as opposed to all of the Martinsville no. 1 core was appropriate is indicated by the near perfect match between the ACE cores of the lower Feltville and Silver Ridge B-1 core in the lower Shuttle Meadow Formation of the Hartford Basin, which is in a deeper water facies and better developed cyclicity (Fig. S3).

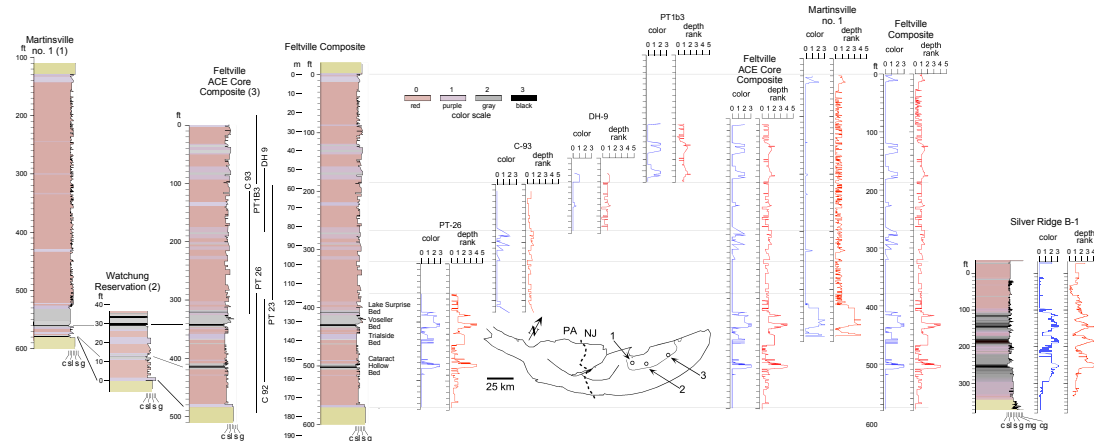


Fig. S3. Construction of the composite Feltville Formation section. Locations are given in **Table S1**. Note the thinning and onlap of the lower Feltville Formation with the ACE core composite closely approximating the proportions of the correlative lower Shuttle Meadow Formation which has much higher amplitude cyclicity as evidenced in the Silver Ridge core (7).

Splicing lower East Berlin Formation into the Towaco Formation. The concept behind the splice is based on the observation that based on the MDC cores, the upper three-quarters of the East Berlin Formation of the Hartford Basin is nearly a perfect match for the Towaco Formation, based on the ACE cores, there is no equivalent to the lower East Berlin in the Newark Basin (Figs. S4 and S5). Instead, the stratigraphic position of the lower East Berlin is occupied by two lava flows of the Preakness Basalt that have no positional or chemical match in the Hartford Basin. There is a very close match between the two lower flows of the Preakness Basalt and Holyoke Basalt (f1 and f2). In both cases, the lowest flow (f1) is not laterally continuous over the basin, which the second flow (f2) is. Apparently, the pillow flow, f3, of the Preakness Basalt is equivalent to the lower gray and black Van Houten cycle in the basal East Berlin.

The same pattern was identified in the Deerfield Basin in which the lower Turners Falls Formation has cyclostratigraphy not seen in the Newark Basin and only two flows, which match f1 and f2 in the Hartford and Newark basins. In all three basins, flow 1 tends to be pillowled, and f2 has unusual but similar paleomagnetic directions that has long suggested they are exactly contemporaneous flows or perhaps the same flow (9,10). The basal Turners Falls Formation also has two weakly expressed Van Houten cycles with laminated purplish red high-stand beds that are in the same position of the lowest gray and black Van Houten cycles of the East Berlin Formation as seen in the MDC cores. It is noteworthy that these two cycles become much less gray laterally and are almost entirely red at Spruce Brook, Berlin, CT (41.601418, -72.737044). We chose to splice the lower East Berlin Formation onto the Towaco Formation ACE cores, because of the higher accumulation rate in the Towaco and higher accumulation rates tend to have less variation in average accumulation rates, based on the quality of the spectra.

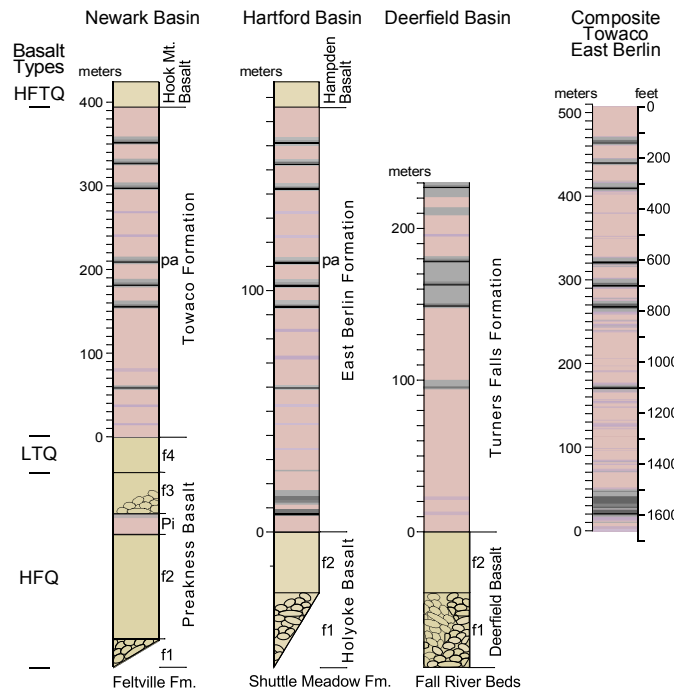


Fig. S4. Conceptual framework for splicing the lower East Berlin onto the base of the Towaco Formation. The composite is from Fig. S5. The circular patterns represent pillowved basalt. The basalt types are from ref. (12) and are: HFQ, high iron, quartz-normative; LTQ, low-titanium Quartz normative; and HFTQ, high-iron, high-titanium quartz normative. f1-f4 are flow 1 through flow 4 of the Preakness, Holyoke, and Deerfield basalts. Pi, is a mappable sedimentary interbed between flows f2 and f3 of the Preakness Basalt. pa, is the Pompton Ash (11), identified in both the Newark and Hartford basins over a distance of 200 km and at 10 sites. The diagonal cutoff of f1 indicates that the flow is not continuous over the area of f2.

The Towaco and Lower East Berlin formations were spiced together by scaling the MDC East Berlin Formation section (cores BD-227A and BD-255) to the lower Towaco Formation (Fig. S5). For fiducials we use the base of the dark mudstones in the lowest of the three middle black-mudstone-bearing cycles (the uppermost of which contains the Pompton Ash), and the lowest of the prominent dark mudstone-bearing cycle in the lower third of the formations. The ratio of the correlative intervals in the Towaco and East Berlin formations, so defined, is 2.860388114, which was used to scale the lower East Berlin Formation section to the Towaco Formation. The top of the composite BD-227A

and BD-255 cores was then spliced onto the correlative part of the Towaco Formation. A check on the scaling is MCD core BD-226.

For the time domain analysis, a different method was used to tune the Feltville Formation compared to the rest of the post-Orange Mountain Basalt formations. Because the Feltville Formation spectrum was not well-resolved, we employed zircon U-Pb radioisotopic constraints from Blackburn et al. (2013) using the dates 201.520 for the Orange Mt. Basalt (from the Palisade Sill) and 201.274 Ma from flow 2 (Preakness Basalt) (12) yielding a duration of 246 kyr for the Feltville Formation. Counting cycles from ref 13, the duration would have been 220 kyr). In contrast, spectra from the Towaco Formation plus basal East Berlin and Boonton formations are well resolved. They were patched together by using the average of the periods of the two prominent peaks in depth rank at the Van Houten cycle-scale in the Towaco-East Berlin (85.97883598 ft) formations to scale the Boonton Formation (62.88819876 ft). The ratio of the average periods is 1.367169638744476. The composite Boonton-Towaco/East Berlin was then scaled to the Feltville Formation by assuming the duration of the period of the average of the two prominent peaks in the composite was 20 kyr. **Fig. S5.** Composite of Towaco and lower East Berlin Formation based on Newark Basin ACE cores of the Towaco Formation (PT-17, PT-16, PT-14, PT-13, PT-12, PT-11, C-103) and Hartford Basin MDC cores of the lower East Berlin Formation (BD-226, BD-227A, BD-225). Locations given in **Table S1**.

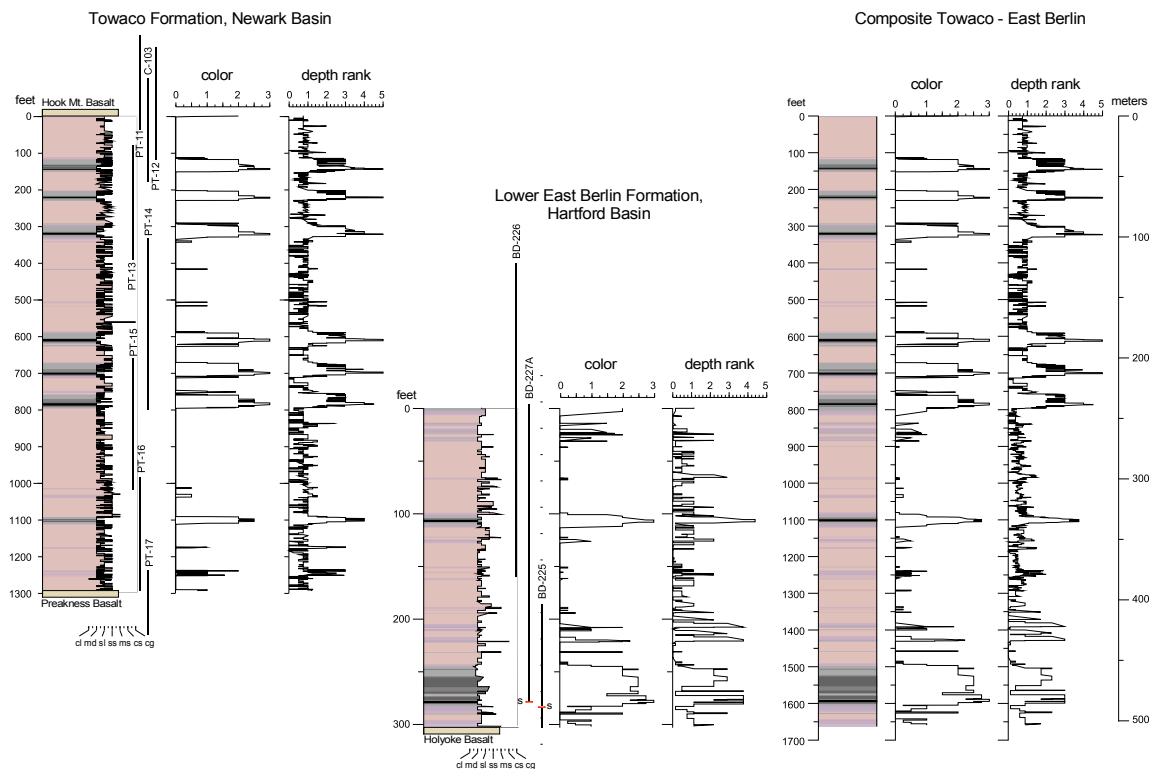


Fig. S5. East Berlin Splice for the Towaco Formation. Depth Rank and color data were averaged in overlap interval with the depth of the East Berlin segment scaled to the Towaco Formation based on the overlapping matching lithological marker beds.

Thickness Wavelets of Newark Hartford Composites

All composite sections were interpolated to 0.4 ft and processed using the Matlab script WAVELET of ref. (14) using the following script parameters: pad = 1, depth series was padded with zeroes; dj = 0.25, 4 sub-octaves per octave; s0 = 3*dt; x axis starts at a scale of 4*0.4 feet; j1 = 11./dj, periods expressed as 11 powers-of-two with dj sub-octaves each; lag1 = 0.72; autocorrelation for red

noise background; and Morlet, was used as the mother wavelet. The results for all the data sets are shown in **Fig. S6**

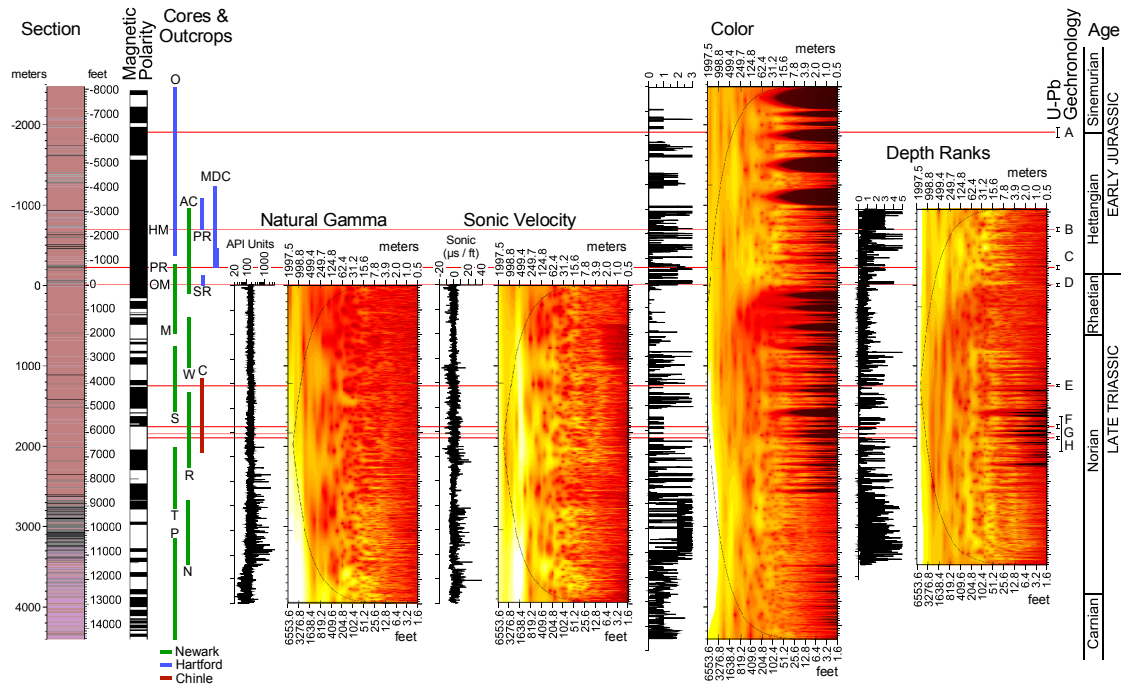


Fig. S6. Evolutive wavelet spectra in thickness of natural gamma (borehole), sonic velocity (borehole), color (core), and depth ranks (core) data Form the Newark and Hartford composit data. Abbreviations of the cores and outcrops are: AC, Army Corps of Engineers cores (Newark Basin); C, CPCP-PNFP-13-1A core, Colorado Plateau; M, Martinsville core and hole (NBCP); MCD, Metropolitan District Commission cores (Hartford Basin (bump is part used here, see SI)); N, Nursery core and hole (NBCP); O, outcrops (Hartford Basin); P, Princeton core and hole (NBCP); PR, Park River cores (Hartford Basin); T, Titusville core and hole (NBCP); R, Rutgers core and hole (NBCP); S, Somerset core and hole (NBCP); SR, Silver Ridge Core (Hartford Basin); Weston Canal core and hole (NBCP). Zircon U-Pb Geochronology are CA-ID-TIMS dates as follows: A, 199.46 ± 0.17 (Hettangian-Sinemurian boundary, Peru – ref. 15); B, 200.916 ± 0.067 (CAMP - 13); C, 201.274 ± 0.032 (CAMP - 13); D, 201.520 ± 0.034 (CAMP - 13); E, 210.08 ± 0.22 (CPCP – ref. 16); F, 213.55 ± 0.28 (CPCP – ref. 16); G, 212.81 ± 1.25 (CPCP – ref. 16); H, 214.08 ± 0.20 (CPCP – ref. 16). Basalts are: HM, Newark Basin basalt flow formations are: HM, Hook Mountain Basalt; OM, Orange Mountain Basalt; PR, Preakness Basalt. Untuned data are given in Excel files `depth_rank_vs_ref_coef_depth.txt`, `sonic_detrend_depth.txt`, `gamma_log_2_depth.txt`, `depth_rank_nbcp+ace_depth.txt`, `color_nbcp+ace+port_depth.txt`.

Comparison Between Depth Rank data and Reflection Coefficient Data

A composite section for depth ranks of part of the Somerset and Rutgers cores from 3726 to 7466 ft (998.5 to 2275.6 m) in the composite NBCP record (Passaic, Lockatong, Stockton) were interpolated to 0.5 ft and processed using the Matlab script WAVELET of ref. 14 using the script parameters as the overall depth sections (see above). The MTM and Blackman-Tukey coherence spectrum were produced using Analyseries. Within the MTM function, we removed the linear trend, used the default confidence vs. resolution (4, 4pi tapers). The f-test results were averaged for display in **Fig. 3**. The coherence spectrum in the Blackman-Tukey spectrum function was also computed using the default values with a Bartlett window, with a bandwidth of 0.00119332, 80% confidence,

and 30% autocorrelation. Non-zero coherence is higher than 0.384442, and coherence and f-test values greater than 0.5 are displayed in **Fig. 3**. The reflection coefficient data were computed using the sonic velocity and density logs following the procedure in ref. (17) and analyzed exactly the same way as the depth rank data.

Cycles Versus Ages and period of the Jupiter-Venus Cycle

Kent et al. (1,4,18) and Kent and Olsen (19) used the lithologically-based members of the Passaic Formation, themselves based on the lithologically-defined McLaughlin cycles to develop the Newark-Hartford APTS. Kent et al. (16) then used these typological McLaughlin cycles to estimate the duration of the long-eccentricity cycle in the Newark Basin NBCP cores (**Table S2**). They used the 8.48 My age difference between the U-Pb-dated tie points at 210.08 Ma for the Black Forest Bed in CPCP PFNP core 1A correlated to Chron E16r corresponding to cycles 20.87–21.60 (centered at cycle 21.24), and 201.6 Ma just below the first Newark Basin CAMP basalt at cycle 0.25. This implies a cycle period of 404 ky which is within 1 ky or 0.25% of the hypothesized 405-ky period (20).

Using a similar typological approach focused on the interval covered by the paleomagnetically-defined correlation interval in the CPCP PFNP core 1A and the NBCP, there is significantly more uncertainty because of the shorter interval (4.0 My). Projecting the four zircon U-Pb dates from CPCP-13-PFNP 1A into the NBCP cores using linear regression ($y=0.06978x+17.01869$, $R^2 = 0.98412$) the McLaughlin cycle has a period of 369 ± 85 ky. If we do not use the one age (i.e., 177Q1: 212.81 ± 1.25 Ma) with a mean that is out of stratigraphic order (although within it when taking into account the analytical uncertainties) the McLaughlin cycle period is 417 ± 14 ky. If we include the Newark Basin CAMP dates from Blackburn et al. (13) the interval is now 13.2 My in duration and the McLaughlin cycle has a period of 401 ± 12 ky.

In order to identify cycles numerically as opposed to typologically, for the pre-basalt flow section, we filtered the untuned NBCP depth rank section (depth ft at delta t of 0.4 ft) with a bandpass filter in Analyseries using a frequency of 0.0042 cycles/ft (same as used for initial tuning steps) and bandwidth 0.002 cycles/foot and a Gaussian window (**Fig. S7**). We identified peak-to-peak cycles at the local maximum value. To project the relative positions of the CPCP zircon U-Pb dates on the NBCP section we linearly regressed the CPCP polarity boundaries (from ref. 16) to the NBCP polarity boundaries in depth (from ref. 19) and used the regression equation ($y=4.37114*M2 + 986.86625$ [in m converted to ft], $r^2=0.96363$) to determine the correlative position of the CPCP zircon U-Pb dates in the NBCP section. The fractional position of the CPCP dates in the NBCP section was then determined from the top down and expressed as a cycle number at a specific depth (e.g., 52Q2 [the Black Forest Bed] has a cycle value of 21.11, an age of 210.08 ± 0.22 , and a position of 4040.8 ft in the NBCP section (**Table S3**).

Table S2: Typologically Identified McLaughlin Cycles.

Sample	CPCP position U-Pb (m)	Projected to Newark Cycle Number	U-Pb Age (Ma)	\pm (Ma)
HM	NA	-1.53	200.916	0.034
PB2	NA	-0.69	201.274	0.032
OMB	NA	0	201.520	0.064
52Q2	56	20.93	210.08	0.220
158Q2	172	29.02	213.55	0.280
177Q1	190	30.28	212.81	1.25
182Q1	195.3	30.65	214.08	1.20

We used a similar approach to identify the cycle position of the zircon U-Pb dates of Blackburn et al., (2013) in the composite ACE-MDC core section (**Table S3, Fig. S7**). Because the

thickness of the cycles identified as the 1330 ft (405.4 m) is so much thicker compared to the average in the rest of the NBCP (~238.1 ft, 72.6 m), the determination of the cycle position in Blackburn et al. (2013) was done separately using a bandpass filter in Analyseries using a frequency of 0.00072 cycles/ft and bandwidth 0.00014 cycles/foot with a Gaussian shape window. This method does NOT rely on the *a priori* identification of cycles or a tuning of cycles to an assumed period and therefore less subjective (Fig. S7).

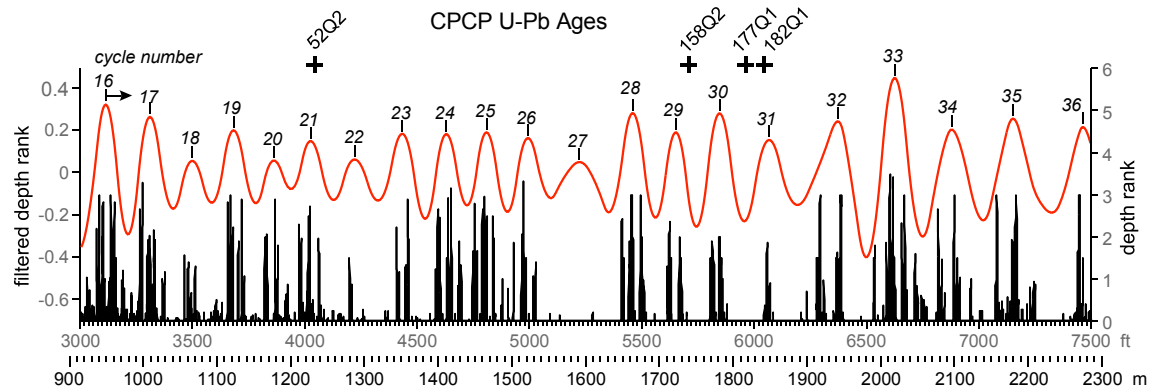


Fig. S7. Filtered depth rank series of NBCP cores overlapping with portion of ages from CPCP13-PFNP-1A core from ref. 16.

Using this numerical method, the long modulating cycle has a period of 365 ± 84 ky using all four CPCP radiotisotopic dates, 413 ± 12 ky using the three CPCP dates that are in stratigraphic order, 398 ± 12 ky using all four CPCP dates and the Newark Basin CAMP dates, and 410 ± 02 ky using the three CPCP dates in stratigraphic order and the Newark Basin CAMP dates. This exercise demonstrates that the CPCP and NPCP dates identify a prominent cycle within a few thousand years of 405 ky regardless of the counting method employed.

Table S3. Numerically Identified Long Eccentricity Cycle

Sample	CPCP position U-Pb (m)	Projected to Newark (m)	Projected to Newark (ft)	U-Pb Age (Ma)	\pm (Ma)	Cycle position
HM	NA	NA	31.7*	200.916	0.034	-1.40
PB2	NA	NA	1332.6*	201.274	0.032	-0.44
OMB	NA	NA	2653.0*	201.520	0.064	0.23
52Q2	56	1231.7	4040.8**	210.08	0.22	21.11
158Q2	172	1738.7	5704.4**	213.55	0.28	29.31
177Q1	190	1817.4	5962.5**	212.81	1.25	30.56
182Q1	195.3	1840.5	6038.5**	214.08	1.2	30.90

*Based on NBCP-ACE-MCD depth rank composite (0-3330 ft)

**Based on NBCP depth rank composite only (Fig. S6).

For Figure 4 of the text, the simple age model for untuned NBCP data using zircon U-Pb CA-ID-TIMS dates from basalt flows in the Newark Basin section, the MTM spectra were produced using Analyseries 2.0 with a default of 6, 4pi tapers.

Comparison of Depth Rank data to Instrumental Chemical Data

The depth rank scale of relative water depth is based on a subjective, although meaningful, classification and ranking of sedimentary facies related to relative water depth and relative permanence of water. We use XRF chemical data acquired using an ITRAX core scanner at LDEO to compare the time series spectral characteristic a sequence of the lower Tumble Falls Member of the Lockatong Formation with depth ranks (**Fig. S8**).

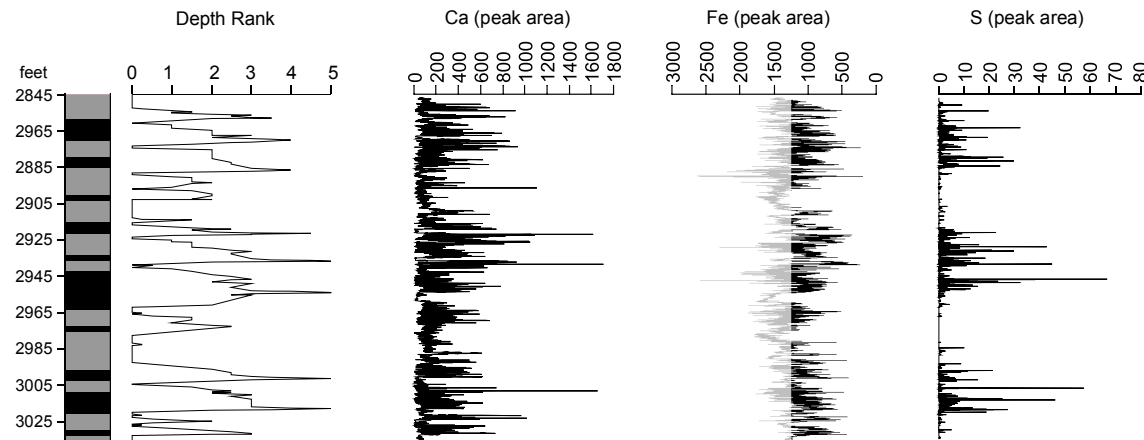


Fig. S8. ITRAX XRF data from lower part of the lower Tumble Falls Member of the Lockatong Formation in the Titusville no. 1 core. Note that the grayed data in the Fe peak area has been clipped for use in the spectra in Figure S9.

All scans were conducted using an Rh tube kept at a constant voltage (30 kv) with a beam area of 22 mm x 100 um. All sections of core were unsplit and scanned over 5 mm intervals with 30 second count times. Output is in the form of peak area, which reflects the relative concentration of each element. The MTM spectra (**Fig. S9**) for depth rank (dr), S, and Ca for the interval scanned from the Titusville core (Analyseries 2.0: 2.7pi, 4 tapers). Ca, S and Fe results reproduce depth rank at lower frequencies consistent with the 100-kyr eccentricity and 25 - 18 kyr climatic precessional cycle but also capture additional, higher-frequency cycles with periods at ~ 10 kyr and ~ 5 kyr. The latter high frequency cycles can be seen in the data (**Fig. S8**). They could be edge effects of redox boundaries at the contacts of contrasting lithologies with different TOC contents, or they could represent actual climate signals in the hemi-precession range. While it would be highly desirable to have such instrumental measurement on the entire Newark-Hartford core data set, this has to yet be accomplished because of the magnitude of the undertaking.

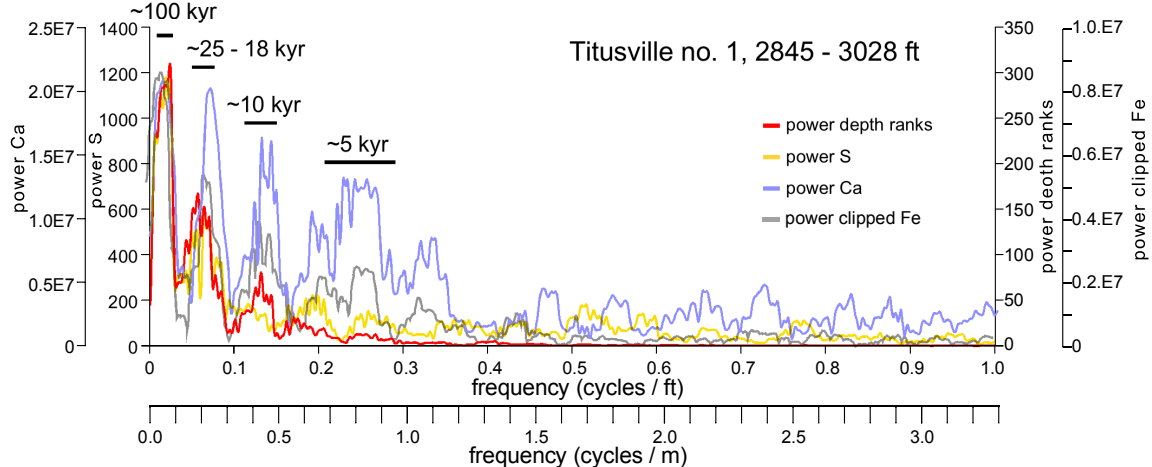


Fig. S9. MTM spectra of ITRAX XRF sulfur, calcium, and iron data compared to depth rank data for the lower Tumble Falls Member of the Lockatong Formation in the Titusville no. 1 core.

Tuning to the 405 ky Jupiter-Venus Cycle

Once we established that the 405 ky cycle is stable from the present at least back into the Triassic and that the overall sequence lacks significant gaps using a simple age model (Fig. 4), it is appropriate to tune the Newark Hartford data to the 405 ky cycle. This was done in a similar procedure to in ref. (21) using just the NBCP Passaic, Lockatong and Stockton data because the accumulation rate is nearly an order of magnitude higher for the younger strata interbedded with and overlying the CAMP flows using the newly compiled data, not that used in ref. (21), although the differences are hardly noticeable. We first filtered and smoothed the color and depth rank data using Analyseries. For filtering, we used a frequency of 0.0044 cycles/ft and bandwidth of 0.002 cycles/ft (Gaussian) which was broad enough to capture most of what we felt was the range of McLaughlin cycle thicknesses in the NBCP data. Smoothing was done with a least-square (Savitzky-Golay) smoothing with a degree 2 polynomial (using the FFT) that was symmetric with 401 points and boundaries with an assumed value of 0. We then averaged the smoothed color and depth rank series (Fig. S10).

We used the averaged smoothed NBCP data to tune the sequence using the spline function in Analyseries. We used the smoothed color and depth rank averaged data to tune to the 405 ky cycle because smoothing makes looser assumptions about the frequency properties in the data (Fig. S10) than filtering. We picked the maximum values for the waves thought to be representative of deepest and most permanent water except where there was some remaining structure such as two very close maxima using the filtered data as a guide. The peaks in the filtered data match nearly perfectly those in the smoothed data. The maxima in the smoothed data were then correlated to the maxima of the 405 ky cycles (Fig. S10). We did not attempt to tune the Stockton Formation below the fluvio-lacustrine Raven Rock member because that part of the sequence seems entirely fluvial.

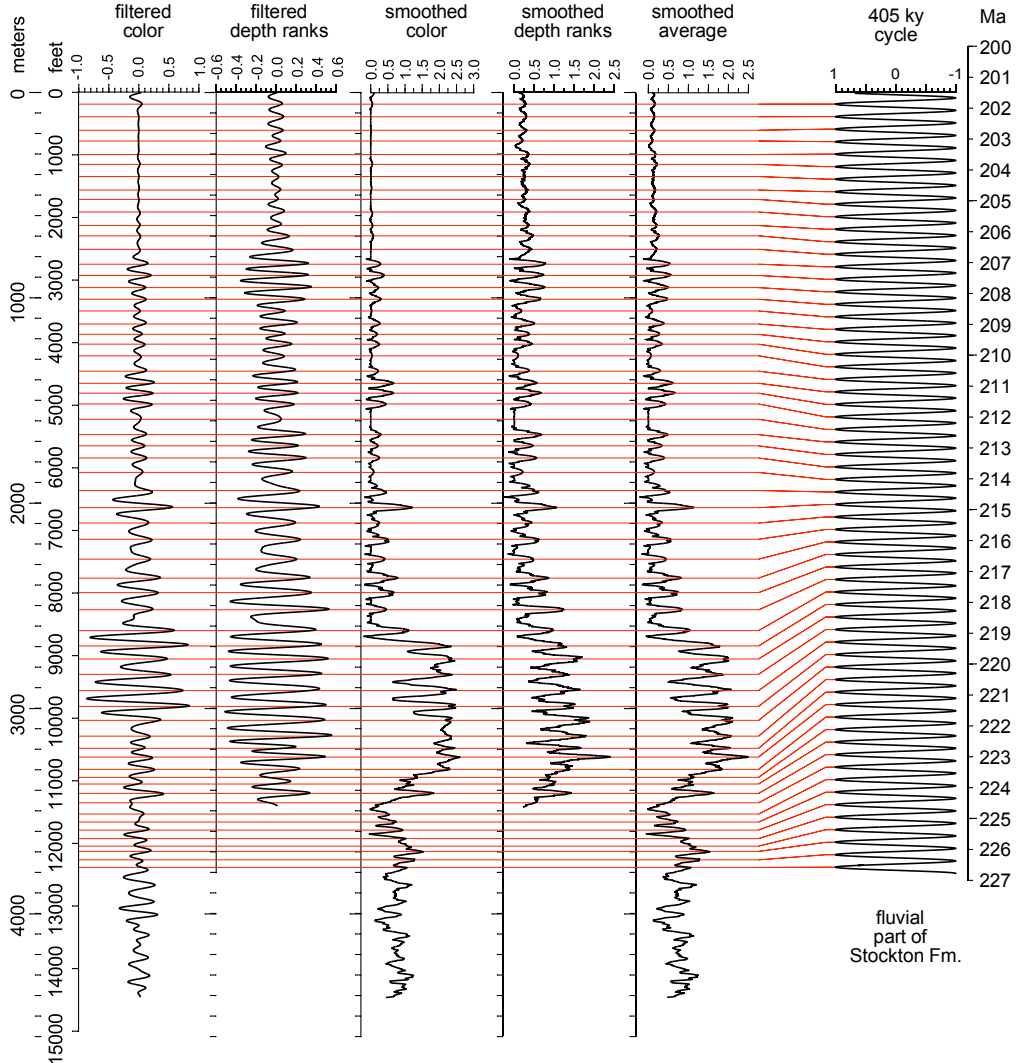


Fig. S10. Tuning the NBCP composite (Passaic through Stockton) to the 405 ky Jupiter-Venus eccentricity cycle.

The resulting tuned NBCP composite time series has the same basic age-depth relationship (**Fig. S11**), as seen previously (1,21), differing only in small details. We can now, however add the Newark ACE, and Hartford data, and obtain the Newark-Hartford composite of accumulation rates (**Fig. S11**). Because of the nearly order of magnitude increase in accumulation rate evident at the onset of CAMP volcanism in the Newark Basin, to which the Hartford data are scaled to, we used the zircon U-Pb age data (13) to scale the Newark ACE and Hartford data to the tuned NBCP data to which it was then concatenated. We filtered the 405-ky-tuned time series with a $1/0.405\text{My}$ filter (2.46914 cycles/My, a bandwidth of 0.5 cycles/My, and a Gaussian shape filter) and mapped the peak values of the 405 ky cycle onto the untuned section in thickness to obtain the age-depth data younger than 201.520 Ma in **Fig. S11**. We smoothed the color and depth rank series using Analyseries 2.0 (Least-square - Savitzky-Golay - smoothing with degree 2 polynomial using FFT; symmetric with 401 points and boundaries: with a value of 0. For the accumulation rate we used the rate data directly from the Splinage function in Analyseries, but use a simple difference for the data younger than 201.520 Ma (**Fig. S11**).

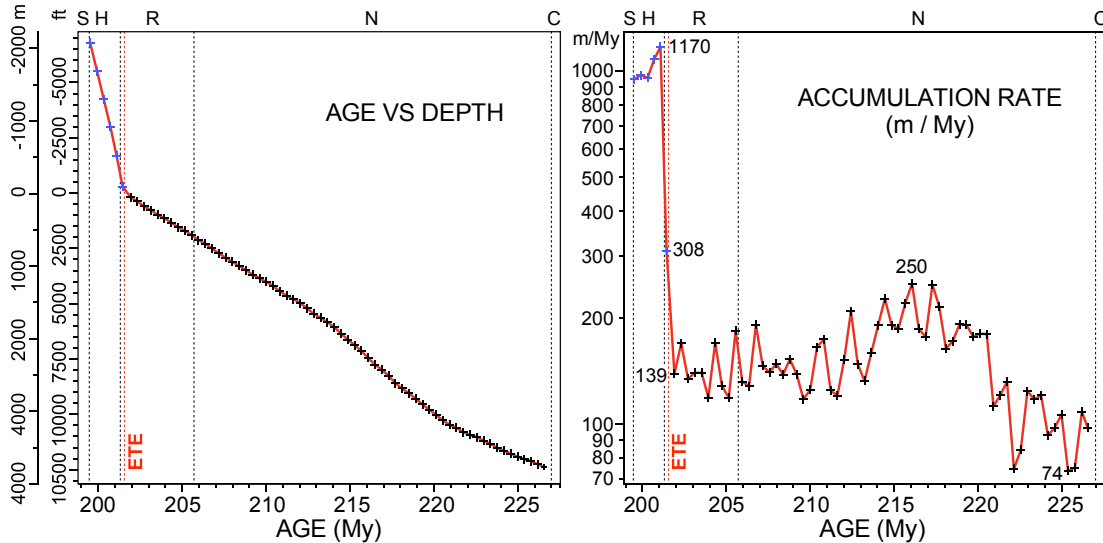


Fig. S11. Age-depth relationships and accumulation rates for the entire cyclical Newark-Hartford data set. Points younger than 201.520 Ma (age of the Orange Mountain Basalt – ref. 13) are shown with blue crosses. The black crosses are from the NBCP Passaic-Stockton data. Selected values of accumulation rate are shown in the accumulation rate graph. Note y-axis (accumulation rate) is on a log scale and that there is a nearly order of magnitude increase in accumulation rate in the data younger than 201.520 Ma (139 m/My to 1170 m/My). The oldest of these points, with an average accumulation rate of 308 m/My, includes a substantial portion of the cycle within the previous much lower accumulation regime. Abbreviations are: C, Carnian Age; ETE, end-Triassic extinction level within the Newark Basin section at 201.564 Ma; H, Hettangian Age; N, Norian Age; S, Sinemurian Age. The age-depth table is given as an Excel file (age_depth.txt).

Wavelets of Newark Hartford Composites in Time

Newark-Hartford 405-ky-tuned gamma, sonic velocity, color, and depth rank data and their wavelet spectra are shown in **Fig. S12**. All composite sections were interpolated to 1 ky and processed using the Matlab script WAVELET of ref. (14) using the following script parameters: pad = 1, depth series was padded with zeroes; dj = 0.25, 4 sub-octaves per octave; s0 = 3*dt; x axis starts at a scale of 3 ky; j1 = 11./dj, periods expressed as 11 powers-of-two with dj sub-octaves each; lag1 = 0.72; autocorrelation for red noise background; and Morlet, was used as the mother wavelet. The results for all the data sets are shown in **Fig. S6**.

For the natural gamma log we transformed the spliced depth data to log2 to reduce the “spikiness” of the data prior to producing the wavelet analysis. The precession index (parameter) (expressed as the standard deviation) series was obtained directly from Analyseries based on the Laskar 2004 (22) solution, and all values less than 0 have been clipped so that the eccentricity signal is revealed. The $\delta^{18}\text{O}$ Megaslice data are from De Vleeschouwer et al. (23). For the figures, we have truncated the displays at the equivalent in time of the base of the depth rank series.

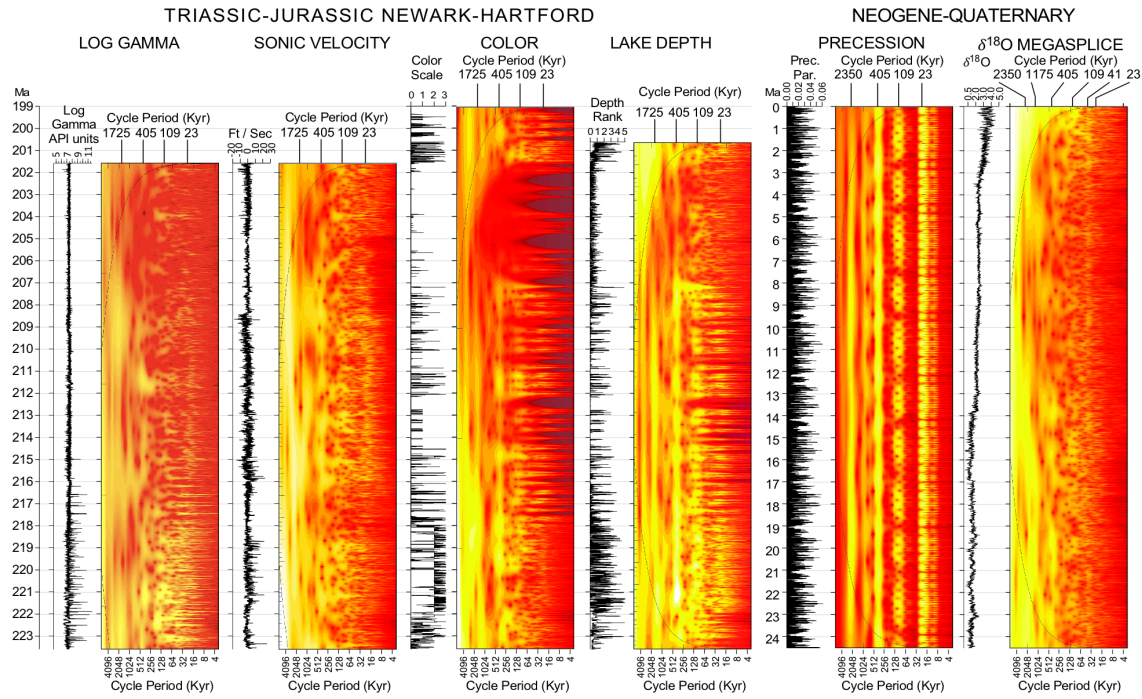


Fig. S12. Wavelet spectra for all of the main 405-kyr-tuned data sets truncated at base of the (Lockatong Formation) compared to the Laskar 2004 solution for the precession parameter (22) and the $\delta^{18}\text{O}$ Megasplice (23) for the same time interval shown for precession. Excel files NBCP_sonic_detrend_tuned_1000yr.txt, NBCP_gamma_log2_tuned_1000yr.txt, B_T_F_P_NBCP_tuned_1000_col.txt, B_T_F_NBCP_tuned_1000yr_dr.txt

Correlation with the Astronomical Solutions

Frequency Analysis of the Newark-Hartford data. In order to establish the correlation with the astronomical solution, once the time scale of the Newark-Hartford (NH) data has been established by tuning it only to the 405 Ky periodic term, a MTM analysis is performed over the full time interval of NH, that is 200.65-225.565 Ma. The main periods that appear in the MTM spectrum can be related to well-known arguments that are the leading terms of the frequency decomposition of the eccentricity of the Earth (see ref. 22, Table 6). The obtained values are displayed in **Table S4**, together with the name of the corresponding arguments (col. 1) that are all of the form g_i-g_j , except $(g_2-g_5)-(g_4-g_3)$ which involve 4 frequencies. In order to verify the values obtained with the MTM analysis, an independent analysis has been used over the same set of data, with a totally different method, that is the method of frequency analysis (FA) that has been developed by Laskar (24,25) to derive precise quasiperiodic approximations from the output of a numerical integration of a dynamical system. This method has a strong theoretical background (25,26) and has been used in the analysis of numerous dynamical systems. While both the MTM and FA methods are ultimately based on Fourier analysis, it is remarkable that the direct use of the frequency analysis algorithm, as given by the "naftab" routine of the freely available TRIP software (<https://www.imcce.fr/Equipes/ASD/trip/>) (see below) provides almost the same result as the one obtained by the MTM method (**Table S4**). The most striking feature of these values, when compared with the equivalent terms of the La2004 (or La2010) solutions (see ref. 22, Table 6), is the very different value of the period of the g_4-g_3 orbital eccentricity term, which amounts to 2373 kyr in the La2004 solution. This argument has a particularly important meaning, as it is in part responsible for the chaotic behavior of the Solar System (see refs. 20,22,24). This unusual feature was observed a by Olsen in 1986 (27), but the new confirmation of the validity of the tuning with the 405 ky astronomical term (16) allows now to retrieve the astronomical signal in the geological data with more confidence.

Table S4: Period and frequencies in the Newark-Hartford (NH) data and in the La2010d solution. Col. 2 (MTM) contains the main periods (in yr) of the NH record, as extracted from the MTM spectral analysis. Col. 3 (FA) are the equivalent terms recovered by a direct Frequency Analysis (refs. 24,25) of the same data. In col. 4 are the main terms of the frequency analysis of the La2010d solution, over the 209 Ma-231 Ma time interval. Cols. 5,6,7, are the corresponding values of the frequencies in arcsec/yr (“/yr) of the same quantities. In col. 1 are the combinations of fundamental secular frequencies (Argument) that are attributed to each periodic term.

	1	2	3	4	5	6	7
	Argument	NH MTM (ky)	NH FA (ky)	La2010d	MTM “/yr	FA “/yr	La2010d “/yr
1	g_4-g_3	1724.63	1747.65	1793.04	0.751	0.742	0.723
2	g_1-g_5	923.04	923.16	957.56	1.404	1.404	1.353
3	g_2-g_1	720.18	719.05	704.98	1.800	1.802	1.838
4	$(g_2-g_5)-(g_4-g_3)$	537.18	527.56	515.09	2.413	2.457	2.516
5	g_2-g_5	405.17	404.97	404.58	3.199	3.200	3.203
6	$(g_2-g_5)+(g_4-g_3)$	336.53	335.13	330.08	3.851	3.867	3.926
7	g_3-g_2	132.53	132.17	132.58	9.779	9.806	9.776
8	g_4-g_2	122.96	123.08	123.47	10.540	10.530	10.496
9	g_3-g_5	99.83	99.78	99.86	12.982	12.989	12.978
10	g_4-g_5	94.43	94.49	94.62	13.724	13.716	13.697

Table S5: Frequency Analysis of the Newark-Hartford data over the whole 200.650-225.565 Ma interval. The terms are searched by decreasing amplitude after removing a running average over 2000 data points (2 My). The first 14 terms are displayed with their frequency (col. 1, in arcsec/yr), period (col. 2 in Ky), The highlighted values are ones are reported in Table S4.

	1	2	3
	Freq (“/yr)	Period (ky)	Amp*1E6
1	3.2	404.97	137615
2	10.53	123.08	55849
3	12.989	99.78	60162
4	9.806	132.17	46960
5	10.67	121.47	45784
6	0.742	1747.65	48026
7	13.716	94.49	46833
8	13.106	98.89	33710
9	13.427	96.52	33678
10	2.457	527.56	28870
11	9.911	130.76	28083
12	12.189	106.32	28329
13	57.274	22.63	30625
14	1.802	719.05	28552

Chaotic diffusion of the Solar System

The Solar System motion is chaotic (24,28). This is due to the presence of several secular resonances (i.e., resonances in the precessing motion of the orbits of the planets), and in particular of the $(s_4-s_3) - 2(g_4-g_3)$ resonance. At present, g_4-g_3 has a period of about 2.4 My, and s_4-s_3 a period of 1.2 My. The associated argument is in libration, like the small oscillations of a pendulum (see ref. 20, Fig. 12). As times goes on, there can be some transition from libration to circulation in this argument, and the $(s_4-$

s_3) and (g_4-g_3) frequencies will drift and no longer be in a 2:1 ratio. This is not observed in the most recent 50 Myr, for which the orbital solution can be retrieved (20) but is expected to have occurred further in the past. Despite some attempts to exhibit such a transition in the geological data (29,30), we are still lacking some convincing evidence that this event actually occurred. We will nevertheless show here how the Newark-Hartford data can be considered as the most convincing evidence of this chaotic diffusion.

The 1.747 My period can be reached by chaotic diffusion of g_4-g_3 . Due to the chaotic nature of the motion of the Solar System (24,28), it is not possible to retrieve its evolution from the only knowledge of the present initial conditions beyond about 60 My (20,31). It is thus not possible to directly compare the NH data to a numerical integration of the Solar System. On the other hand, although it is not possible to retrieve the precise solution of the Solar System, it is possible to search for its possible behavior in the past. Indeed, any numerical integration extending in the past beyond 60 Myr will only show one of the possible paths for the Solar System orbital evolution. In **Fig. 7B**, we plot the past evolution of the g_4-g_3 period for 13 different orbital solutions that were generated with a very accurate model of the Solar System, with initial conditions and parameters that are close to our most precise determinations. One of these solutions is the widely used La2004 solution (22), 7 of them are listed in Table 2 of (22), and the 5 remaining ones were generated as variants of these 7 solutions, with minor modifications of the model or initial conditions. The reader should refer to refs. 22 and 20 for a precise description of the models and methods used to obtain these numerical solutions. The g_4-g_3 term is very sensitive so small drift of the solution due to chaotic diffusion. Over the first 40 My, all solutions behave the same way. Then, the older solution La2004 (in bold red in **Fig. 7**) slightly differs from the others that are all close to the various La2010 variants. These solutions are still very close up to 50 Myr, and then differ in a large extend. This divergence of path can be considered as an illustration of the impossibility to make a prediction beyond 60 My. Their variety of behavior illustrates the extent of the possibilities for the past evolution of our Solar System. Specifically, in **Fig. 7B**, the value 1747 kyr of the g_4-g_3 period is represented by the horizontal green line.

Among the 13 solutions, 4 go below the 1747 ky period line, and 4 come very close to it. In order to test how much the Newark-Hartford data can be compared to the astronomical solution, we have thus selected among these 13 orbital solutions one of them and a time interval where the g_4-g_3 period will be close to the 1747 ky value during a time interval that is close to the extent of the NH data. A good example is thus given by the La2010d solution from (20) in the 209-231 Ma time interval. The largest 10 periodic terms of the eccentricity solution of La2010d over 209-231 Ma, obtained by frequency analysis (24,25) are displayed in **Table S6**, and reported in **Table 3**, col. 4. In the following and in the main text, we will call the part of the solution La2010d over the time interval 209 - 231 Ma, La2010d*, while La2010d will represent the same solution in the most recent 0-20 Ma time interval. The numerical solution comprises all planets and all variables. All fundamental frequencies are thus easily identified, and the corresponding combinations of frequencies (**Table S6**, col. 4) are recognized without ambiguity (see also ref. 22, Table 6). In the Earth eccentricity La2010d* solution, the g_4-g_3 is the 10th term in amplitude, with a 1793 ky period, very close to the 1747 ky period observed in the FA of the NH data. All terms that are highlighted in **Table S6** are reported in **Table S4**, col. 2 and col. 5.

Table S6: Frequency analysis of the eccentricity of the Earth in the La2010d solution over the 209-231 Ma time interval. In addition to the constant term, the 10 periodic terms of larger amplitude are given with their frequency (col. 1) in arcsec/yr ("/yr), period (col. 2 in ky), and associated argument, given as a combination of the fundamental secular frequencies of the Solar System. The highlighted values are reported in Table S4.

	1	2	3	4
	Freq "/yr	Period (ky)	Ampl*1E6	Argument
	0.000		27483	
1	3.203	404.58	5249	g_2-g_5
2	12.978	99.86	3705	g_3-g_5
3	9.776	132.58	2894	g_3-g_2
4	13.697	94.62	2125	g_4-g_5
5	13.853	93.56	1349	
6	10.496	123.47	1282	g_4-g_2
7	13.971	92.77	1226	
8	1.353	957.56	1211	g_1-g_5
9	10.267	126.24	1196	$g_3+g_5-2g_1$
10	0.723	1793.04	1129	g_4-g_3

Determination of the secular frequencies from the Newark-Hartford data. In Table S4, only combinations of frequencies are reported, and not the individual frequencies, g_i . We can nevertheless recover these frequencies with minimal assumptions. This can be considered as a critical test showing that we are actually recovering the eccentricity signal in the NH data.

The NH data has been tuned to the $g_2 - g_5$ 405 ky term which cannot be used for confirmation of the validity of the results. The g_5 frequency is extremely stable (e.g., ref. 20, Table 6). We will thus assume that its value has not changed significantly over the past 250 Ma, which is indeed observed when comparing the g_5 value in La2010d* and in La2010a (note that La2010d* is over 209-231 Ma, while La2010a was analyzed over 0-50Ma). As g_2-g_5 was kept fixed, g_2 also has not changed from its La2010a value (**Table 3**, row 5), but this is expected as g_2-g_5 has been used for the tuning. However, this is still a check of the validity of the tuning and spectral analysis method.

Now comes the most interesting part. Using only the constancy of the g_5 term, we can recover the g_1 , g_3 and g_4 frequencies from the terms $g_1 - g_5$, $g_3 - g_5$, and $g_4 - g_5$ obtained from the NH data either by MTM method (**Table 3**, col. 3) or by Frequency Analysis (**Table 3**, col. 4) and are highlighted in green. The recovered frequencies are close to the nominal La2010a actual values, but they are even closer to the La2010d* values (**Table 3**, col. 6). The most striking example are the g_3 and g_4 frequencies. Using frequency analysis (FA), their recovered values are 17.246 "/yr and 17.973 "/yr. They are not far from the La2010a values, but extremely close to the La2010d* ones (the differences FA-La2010d* are in col. 5). This solution has been selected on the basis of its g_4-g_3 value, so we expect to recover a close value for $g_4 - g_3$, but here, the individual values of the frequencies also matches the La2010d* values. Moreover, this is also a clue that our assumption that these two terms correspond to $g_3 - g_5$ and $g_4 - g_5$ is correct.

It is thus remarkable that although the NH data is tuned only to the $g_2 - g_5$ term (and thus, as g_5 is constant, on g_2), we have retrieved all three values of g_1 , g_3 , g_4 , all extremely close to the values from La2010d*.

Now that we have all five frequencies g_1 , g_2 , g_3 , g_4 , g_5 , we can use the 5 remaining terms (highlighted in blue in **Table 3**) to check some additional consistency relations by computing the corresponding frequency combinations. The differences with the observed values are given in col. 5, respectively for FA. All together, we can consider that we have one constant (g_5), one tuned parameter

(g_2) , one chosen value for (g_4-g_3) , and given these, 7 parameter frequencies are independently recovered with extreme accuracy (**Table 3**, col.5).

Consistency Check Using Difference Frequencies of Short Orbital Eccentricity

Although the information is already mostly imbedded in Table 3 we can look at the constancy between the spectral frequencies in a different way. Because secular frequencies $(g_1 - g_5, g_2 - g_1, \text{etc.})$ are difference frequencies of the fundamental secular frequencies $(g_1, g_2, \text{etc.})$, the system of observed orbital eccentricity frequencies are overdetermined due to the same secular frequencies appear in both low and high orbital eccentricity frequencies. Therefore if the major frequencies observed by MTM analysis or FA reflect true orbital values, most of the long eccentricity, Grand Cycles should be difference frequencies of the frequencies of the short eccentricity cycles. That this is in fact the case is shown below (**Table S7**).

Table S7: Comparison of the observed orbital eccentricity grand cycles (red) from the MTM or FA results with those calculated (bold) from differences among pairs of the observed short eccentricity cycles from the MTM or FA results. Note that the $(g_4 - g_5) - (g_3 - g_2)$ and $(g_3 - g_5) - (g_4 - g_2)$ periods are the side lobe periods from the modulation of the $g_2 - g_5$ cycle by the $g_4 - g_3$ cycle, that is equal to $(g_2 - g_5) - (g_4 - g_3)$ and $(g_2 - g_5) + (g_4 - g_3)$, respectively.

		FA RESULTS									
		g ₃ -g ₂		g ₄ -g ₂		g ₃ -g ₅		g ₄ -g ₅			
		132.53	132.17	123.08	123.08	99.78	99.78	94.49	94.49	132.17	g ₃ -g ₂
MTM RESULTS	g ₃ -g ₂	132.53		1789.60	1747.65	407.16	404.97	331.44	330.08	132.17	g ₃ -g ₂
	g ₄ -g ₂	122.96		1702.81	1724.63	527.08	527.56	406.78	404.97	123.08	g ₄ -g ₂
	g ₃ -g ₅	99.83		404.60	405.17	530.70	537.18	1782.27	1747.65	99.78	g ₃ -g ₅
	g ₄ -g ₅	94.43		328.47	336.53	406.98	405.17	1745.73	1724.63	94.49	g ₄ -g ₅
		132.53		122.96	122.96	99.83	99.83	94.43	94.43		
			g ₃ -g ₂		g ₄ -g ₂		g ₃ -g ₅		g ₄ -g ₅		
MTM RESULTS											FA RESULTS

A Statistical Test.

We can ask if a random set of frequencies in the geological signal could be mistaken for a correlation to the astronomical signal. In other words, how probable is the correspondence we have found between the geological analysis and the astronomical solution? For this we take into account that the 7 terms were selected among the 12 first terms given by the frequency analysis of the NH data (we do not take into account the g_2-g_5 term that was used to tune the data or the g_4-g_3 term used to select the orbital solution). We consider thus the 7 terms h_i of the astronomical solution, and 12 frequencies k_j , randomly chosen in the $[0:20/\text{yr}]$ interval with a uniform distribution. As an evaluation of the proximity of the data to the astronomical solution, we compute the minimal value of the root mean square

$$s = \sqrt{\sum_{\{i=1..7\}} \frac{(h_i - k_i)^2}{7}}$$

where (k_i) $i = 1, \dots, 7$ are taken among the 12 k_j frequencies. We then compute the probability for this value to be lower than the value $s_0 = 23 \text{ mas/yr}$ (milliarcsec/yr) obtained with the NH data (**Table 3**, col. 5). As the expected probability is low, we took 33 billion draws and each time computed the minimal distance of the random frequencies to the astronomical ones. The resulting repartition function is given in **Fig S13** in red. The assumption that the 7 frequencies are randomly picked among 12 is somewhat excessive, as we can see in **Table S5** that the selected terms are always the largest terms in amplitude, close to a given frequency. We have thus made the same experiment with 28 billion draws of 7 frequencies in the $[0.20/\text{yr}]$ interval. The repartition function is plotted in blue in **Fig. S13**.

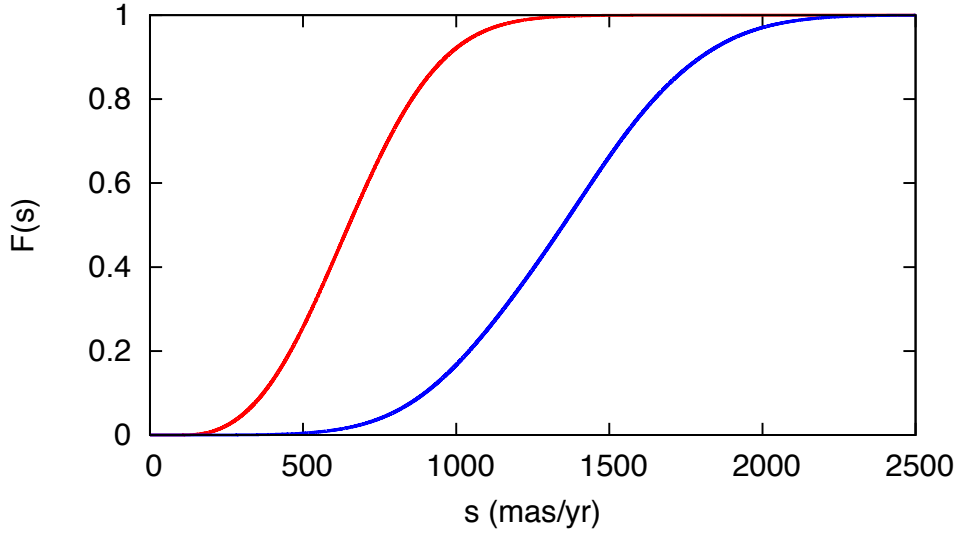


Fig. S13: Repartition function $F(x)$ of the minimal distance of a random draw of 12 frequencies to the 7 main astronomical frequencies (red). The probability to find a result below 500 mas/yr is about 20%. The blue curve is the same repartition function for a draw of 7 frequencies.

The distance value $s_0 = 23$ mas/yr we have in the present study is so small that we need to make an enlargement of the **Fig S13**, which is given in **Fig. S14**. The \log_{10} of $F(s)$ is given in term of the distance (s), for the low values of (s).

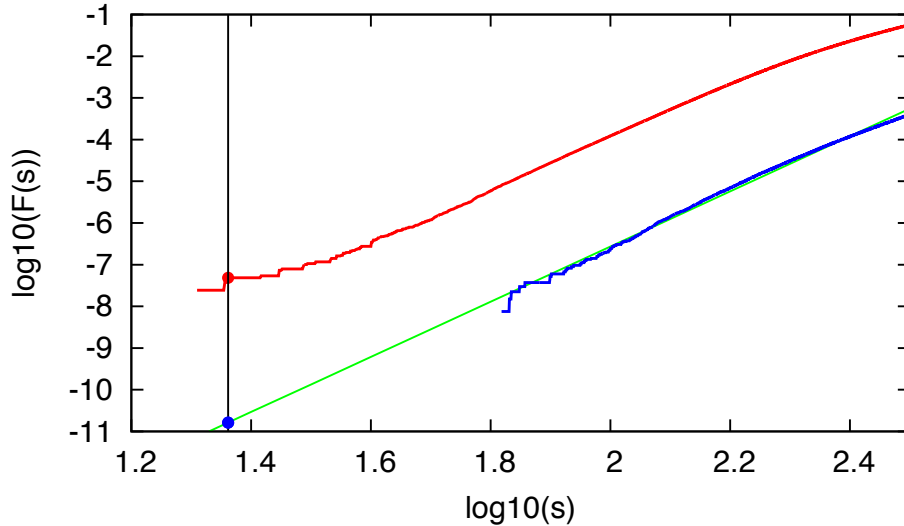


Fig. S14: Decimal logarithm of the repartition function of the distance (s) to the astronomical solution for a random draw of 12 frequencies (in red) or 7 frequencies (in blue) in the [0:20"/yr] range. The vertical line is the $s_0 = 23$ mas/yr value observed with the NH data. For the 7 frequencies experiment, the probability to be closer than s_0 is so low that we linearly extrapolated (in green) to find the expected probability value (about 10^{-11}).

We thus see in **Fig. S14** that the probability that the very good match we find for the NH data to the astronomical solution, is due to pure chance, is less than 5×10^{-8} when considering that the seven frequencies were selected among 12, and on the order of 10^{-11} when only 7 seven frequencies are considered.

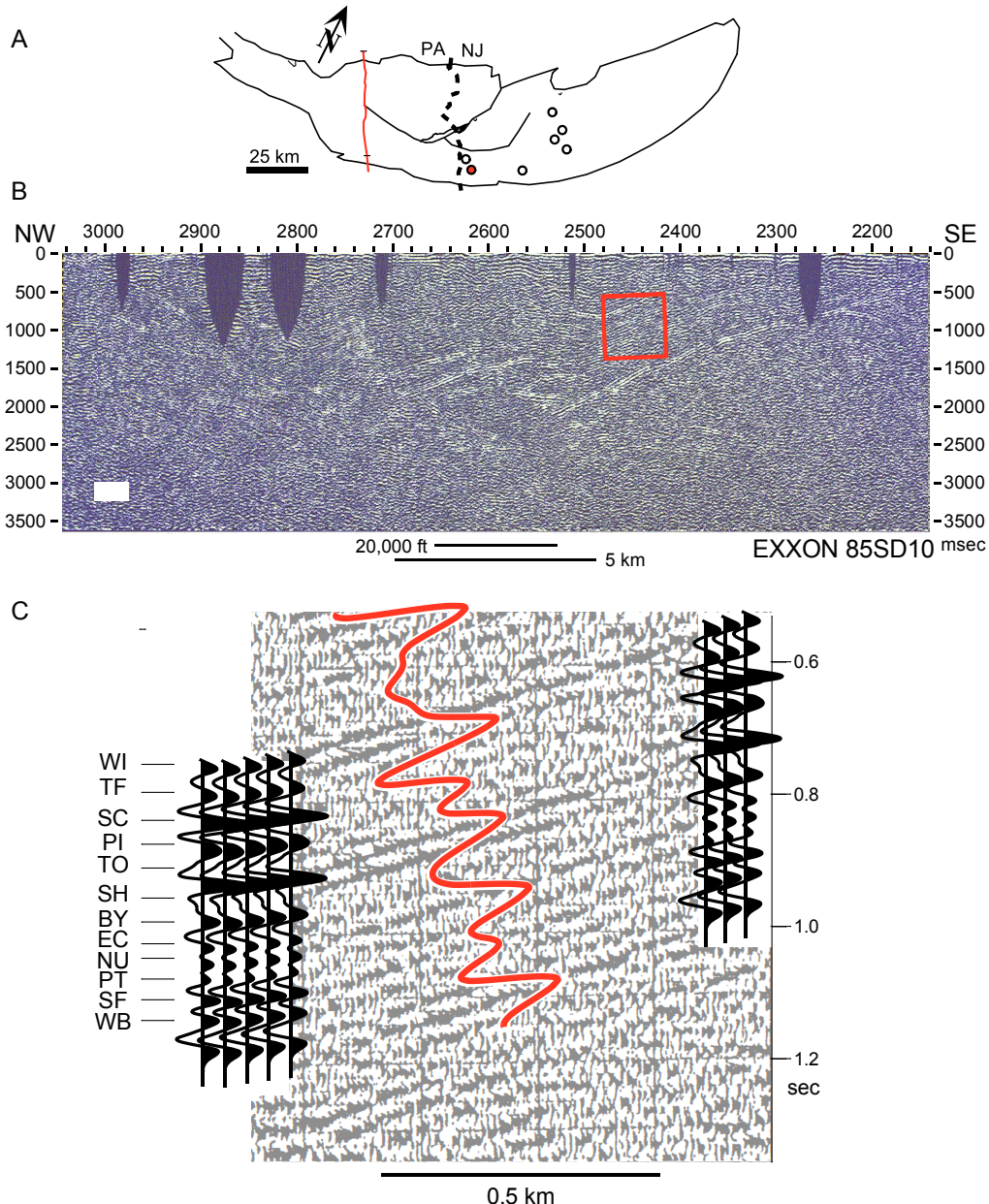


Fig. S15. Example of seismic expression of Grand Cycles modified from ref. (17). A, Outline map of the Newark basin showing the position (red line) of Exxon 85SD10. Small black ticks on red line show portion shown in B. B, Portion of Exxon seismic line 85SD10 showing the half graben geometry of the basin and position of the close up shown in C (red box). Seismic line image is screen shot of CRT display, vintage 1994. C, Synthetic seismic traces (black) of Nursery core tied to portion of Exxon seismic line in B that spans the Lockatong Formation, superimposed on which is the g_4-g_3 , g_1-g_5 , and g_1-g_2 components of the eccentricity signal of the Newark-Hartford data from 216.0 to 223.8 Ma. Abbreviations of the members of the Lockatong Formation from the Nursery core are: WI, Walls Island Mb.; TF, Tumble Falls Mb.; SC, Smith Corner Mb.; PI, Prahls Island Mb.; TO, Tohickon Mb.; SH, Skunk Hollow Mb.; BY, Byram Mb.; EC, Ewing Creek Mb.; EC, Ewing Creek, Mb.; NU, Nursery Mb.; PT, Princeton Mb.; SF, Scudders Falls Mb.; WB, Wilburtha Mb.

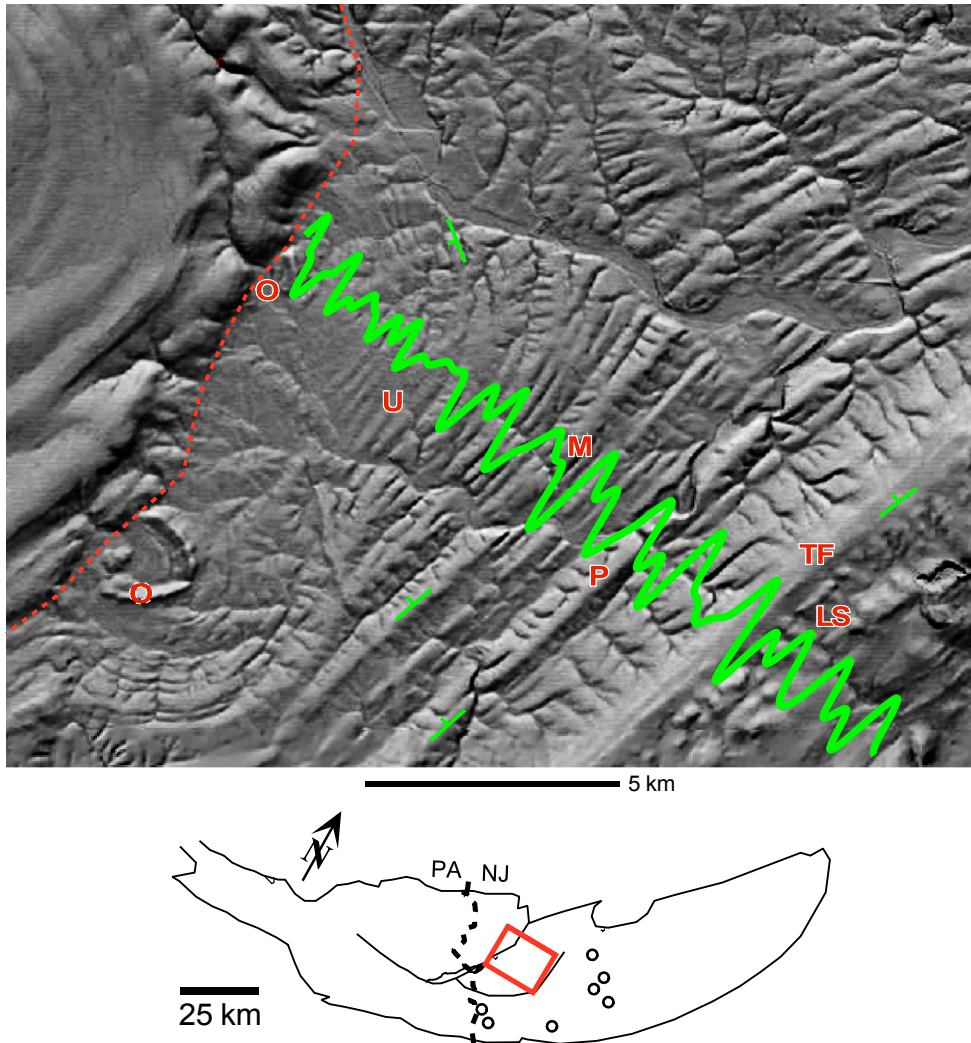


Fig. S16. Digital Elevation Model from National Map Viewer (32) in the central fault block of the Newark Basin (red box in outline map) with superimposed g_4-g_3 , g_1-g_5 , and g_1-g_2 components of the eccentricity signal (green wiggle) of the Newark-Hartford data (Passaic-Lockatong only). Peaks in eccentricity occur at units underlying the most prominent ridges because they are more highly cemented eccentricity graph follows axis of the Flemington syncline beginning at the Orange Mountain Basalt (O) at Flemington, NJ. The narrowest ridges are the 405 ky Jupiter-Venus cycles. Abbreviations are: L, LS, CAMP diabase intrusion Lambertville Sill in the Lockatong Formation; M, Metlars Member (Passaic Fm.); O, Orange Mountain Basalt; P, Perkasie Member (Passaic Fm.); TF, Tumble Falls Member (Lockatong Fm.); U, Ukrainian Member (Passaic Fm.). Small circles in map are locations of NBCP cores. Note that the younger part of the graphs has been compressed in this image to account for the higher dips approaching the Orange Mountain Basalt in the Flemington Syncline.

Seismic and Outcrop Expression of Grand Cycles

Lithologic expression involving grand cycles includes alternation of long sequences of heterogenous lithologies with degrees of cementation that influence both the density and the velocity of sound in the rocks with a scale large enough to be seen in seismic reflection profiles. Synthetic seismograms of industry boreholes and the NBCP core holes indicate that the 405 Jupiter-Venus cycle will be the smallest cyclical feature plausibly imaged by the 1980s vintage Newark Basin industry

seismic profiles. The synthetic seismograms suggest that the Grand Cycles will be a prominent feature of the seismic profiles and that seems to be the case (**Fig. S15**). The most prominent reflection couplets occur at eccentricity maxima which have the deepest lacustrine sequences and the most cemented shallow water intervals.

The same strong cementation of the shallow water units associated with the thickest black shales deposited during times of highest eccentricity and greatest precessional variability evidently results in topographic ridges in the northwesterly dipping and erosionally truncated units (**Fig. S16**). The topography therefore expresses the grand cycles with the smallest units with a distinct topographic expression being the g_5-g_2 405 ky cycles, and larger ridges and clusters of very prominent smaller ridges marking out the lower frequency Grand Cycles. This association of the eccentricity peaks with the largest topographic ridges is validated by detailed mapping (2) and outcrop correlation, confirmed by paleomagnetic polarity correlation to the NBCP cores (18). These are also the members with formal names in the Passaic Formation as well as tending to be the most fossiliferous units. Image is a screen shot of a CRT display, vintage 1994. C, Synthetic seismic traces (black wiggles) of Nursery core tied to portion of Exxon seismic line in B that spans the Lockatong Formation, superimposed on which is the g_4-g_3 , g_1-g_5 , and g_1-g_2 components of the eccentricity signal of the Newark-Hartford data from 216.0 to 223.8 Ma.

TRIP file

TRIP file used to recover **Table S5** is given below.

```
/*
trip_fanh.t : trip file for the
Frequency analysis of the NH data (to recover the S5 Table of
The Geological Orrery: Mapping Chaos in the Solar System
by P.E. Olsen, J. Laskar, D.V. Kent, S.T. Kinney, D.J. Reynolds, J. Sha, and
J.H. Whiteside: PNAS, 2018)
To use this file :
- download and install the TRIP software (https://www.imcce.fr/trip)

put in the same folder the data (B_T_F_NBCP_tuned_1000yr_dr.txt) and this file
- in a unix or mac terminal
A) go to this folder
B) type
> trip trip_fanh.t

- On Windows, the most easy is to use TRIP STUDIO that is installed together
with TRIP console
In TRIP STUDIO in the upper left of the window
File -> Run : and then select the file trip_fanh.t

you are then in interactive mode within TRIP. To exit type
> quit; or Ctrl C

For all details, refer to the TRIP documentation.
(c) J. Laskar, 11/10/2018
*/


macro anadat{
// main routine
// load file
// smooth
// frequency analysis

file="B_T_F_NBCP_tuned_1000yr_dr.txt";
```

```

vnumR t,dr;
read(file,[3::],t,dr);

sdr=%smooth3[2000,dr];
dr2=dr-sdr;

_naf_dtour =360*3600 ; // units of frequencies are in arcsec/yr
NTERM=28;           // number of terms to search for
%subnafR [ t, dr2, NTERM];

try{
  plot(t/1E6,dr,"notitle w l");
  replot(t/1E6,sdr,"notitle w l lw 3");
}catch {
  msg "";
  msg " WARNING!!! You need to install gnuplot to see the plots ";
};

};

macro subnafR[_tt,_xx,NTERM]{
// frequency analysis ( wrapper for naftab)
// _naf_dtour is by default 360*3600 (units are arcsec)
private _ALL; _quiet on;
vnumR tf,trx,tryy;
vnumC za;
_naf_icplx=0$;
_step = (_tt[2]-_tt[1])$;

_yy=_xx*0$;
naftab(_xx,_yy,za,tf,size(_xx),_step,_tt[1],NTERM,trx,tryy)$

P=_naf_dtour/tf;
ang=arg(za)/PI*180;
writes("%22.6f %12.3f %12.6f %10.3f\n",tf,P,abs(za),ang);
};

///////////////////////////// additional routines for smoothing

macro smooth2[_pas,_xx]{
/*****************************************/
/* smoothing by running average over _pas,_pas */
/*****************************************/
private _ALL; _quiet on;
_sxx=_xx;
_siz=size(_xx);
for n=1 to _pas{
  _sxx[n] = sum(_xx[1:n+_pas])/(_pas) $;
}

for n = _pas+1 to _siz-_pas {
  _sxx[n] = sum(_xx[n-_pas:n+_pas])/(_pas*2+1) $};
for n = _siz-_pas+1 to _siz {
  _sxx[n] = sum(_xx[n-_pas:_siz])/(_siz-n+_pas+1) $};

return(_sxx);
};

macro smooth3[pas,xx]{
/*****************************************/
/* smoothing by running average over _pas,_pas */

```

```

improved version on the edges by least square extrapolation of the data */
/********************************************* */

private _ALL; _quiet on;
siz=size(xx);
/* add data on both sides */
_AT =1,pas;

_DT0=xx[1:pas];
ab=%least[_AT, _DT0];
_ATn = -pas+1,0;
_AT0=ab[1]*_ATn + ab[2];

_DT1=xx[siz-pas+1:siz];
ab=%least[_ATn, _DT1];
_AT1=ab[1]*_AT + ab[2];

_gxx=vnumR[_AT0:xx:_AT1];

_sgxx=%smooth2[pas,_gxx];
_sxx=_sgxx[1+pas:siz+pas];
return(_sxx);
};

/********************************************* */
/*return least square determination of a and b such as TY=a*TX+b
*/
macro least[TX,TY]{
private _ALL;_quiet on;
__S=size(TX)$
__SX=sum(TX)$
__SY=sum(TY)$
__SXY=sum(TX*TY)$
__SXX=sum(TX*TX)$
__DEL=__S*__SXX-__SX*__SX$;
a = (__S*__SXY-__SX*__SY)/__DEL$;
b = (__SXX*__SY-__SX*__SXY)/__DEL$;
return(a,b);
};

%anadat;

```

Captions for datasets S1 to S9

Dataset S1: File name S1_B_T_F_NBCP_tuned_1000yr_dr.txt is an EXCEL.txt file of depth rank data from the concatenated and scaled (to the Rutgers no. 1 core) from the NBCP, ACE plus MDC, Park River and Silver Ridge B1 cores. In millions of years from present in 1000 year increments, tuned to the 405 ky cycle.

Dataset S2: File name S2_B_T_F_P_NBCP_tuned_1000_col.txt is an EXCEL .txt file of color data from the concatenated and scaled (to the Rutgers no. 1 core) from the NBCP, ACE plus MDC, Park River and Silver Ridge B1 cores, and Portland Formation outcrops. In millions of years from present in 1000 year increments, tuned to the 405 ky cycle.

Dataset S3: File name S3_NBCP_gamma_log2_tuned_1000yr.txt is an EXCEL .txt file of natural gamma ray data from the concatenated and scaled (to the Rutgers no. 1 core) from the NBCP coreholes. In millions of years from present in 1000 year increments, tuned to the 405 ky cycle.

Dataset S4: File name S4_NBCP_sonic_detrend_tuned_1000yr.txt is an EXCEL .txt file of sonic velocity data from the concatenated and scaled (to the Rutgers no. 1 core) from the NBCP coreholes. In millions of years from present in 1000 year increments, tuned to the 405 ky cycle.

Dataset S5: File name S5_B_T_F_NBCP_dr_depth.txt is an EXCEL .txt file of depth rank from the NBCP, ACE plus MDC, Park River and Silver Ridge B1 cores in depth coordinates in 0.4 foot (decimal foot original drillers units) increments.

Dataset S6: File name S6_S2_B_T_F_P_NBCP_color_depth.txt is an EXCEL .txt file of color data from the concatenated and scaled (to the Rutgers no. 1 core) from the NBCP, ACE plus MDC, Park River and Silver Ridge B1 cores, and Portland Formation outcrops in depth coordinates in 0.4 foot (decimal foot original drillers units) increments.

Dataset S7: File name S7_NBCP_gamma_log_2_depth.txt is an EXCEL .txt file of natural gamma ray data from the concatenated and scaled (to the Rutgers no. 1 core) from the NBCP coreholes in depth coordinates in 0.4 foot (decimal foot original drillers units) increments.

Dataset S8: File name S8_NBCP_sonic_detrend_depth.txt is an EXCEL .txt file of sonic velocity data from the concatenated and scaled (to the Rutgers no. 1 core) from the NBCP coreholes in depth coordinates in 0.4 foot (decimal foot original drillers units) increments.

Dataset S9: File name S9_somerset_rutgers_depth_rank_vs_ref_coef_depth.txt is an EXCEL .txt file of depth rank and reflection coefficient data from contiguous portions of the Somerset and Rutgers NBCP cores (depth rank) and coreholes (reflection coefficient) concatenated and scaled to the Rutgers core in depth coordinates of 0.5 foot (decimal foot original drillers units) increments.

References

1. Kent DV, Olsen PE (2008) Early Jurassic magnetostratigraphy and paleolatitudes from the Hartford continental rift basin (eastern North America): Testing for polarity bias and abrupt polar wander in association with the Central Atlantic Magmatic Province. *J Geophys Res* 113:B06105.
2. Olsen PE, et al. (1996) High-resolution stratigraphy of the Newark rift basin (early Mesozoic, eastern North America). *Geol Soc Am Bull* 108:40–77.
3. Olsen PE, et al. (2018) Colorado Plateau Coring Project, Phase I (CPCP-I): A continuously cored, globally exportable chronology of Triassic continental environmental change from Western North America. *Sci Drill In Review*.
4. Kent DV, Olsen PE, Muttoni G (2017) Astrochronostratigraphic polarity time scale (APTS) for the Late Triassic and Early Jurassic from continental sediments and correlation with standard marine stages. *Earth Sci Rev* 166:153–180.
5. Steinen, R et al. (2015) Stratigraphic observations on cored boreholes in the Mesozoic Hartford basin, Hartford, Connecticut. *Geol Soc Am, Abstr Progs* 47(3):54.
6. Department of the Army New England Division (1976) *Water Resources Development Project, Park River Local Protection, Connecticut River Basin, Hartford, Connecticut, Design Memorandum No. 9, Site Geology, Foundations, Concrete Materials and Detailed Design of Structures*. Corps of Engineers, Waltham, Mass., 177 p.
7. Whiteside JH, et al. (2011) Pangean great lake paleoecology on the cusp of the end-Triassic extinction. *Palaeogeogr Palaeoclimatol Palaeoecol* 301(1-4):1-17.
8. Olsen PE, Schlische RW, Fedosh MS (1996) 580 ky duration of the Early Jurassic flood basalt event in eastern North America estimated using Milankovitch cyclostratigraphy. *The Continental Jurassic* Morales M, ed (Museum of Northern Arizona Bulletin 60), pp. 11–22.
9. Irving E, Banks MR (1961) Paleomagnetic results from the Upper Triassic lavas of Massachusetts. *J Geophys Res* 66(6):1935-1939.
10. Prevot M, McWilliams M (1989) Paleomagnetic correlation of Newark Supergroup volcanics. *Geology* 17: 1007-1010.
11. Olsen PE, Philpotts AR, McDonald NG, Steinen RP, Kinney ST, Jaret SJ, Rasbury ET (2016) Wild and wonderful implications of the 5 mm Pompton Ash of the Hartford and Newark basins (Early Jurassic, Eastern North America). *Geo Soc Am, Absts Prog.*, Northeast Sect 48(2), doi: 10.1130/abs/2016NE-272509.
12. Tollo RP, Gottfried D (1992) Petrochemistry of Jurassic basalt from eight cores, Newark Basin, New Jersey: Implications for the volcanic petrogenesis of the Newark Supergroup. *Eastern North American Mesozoic Magmatism*, Puffer JH and Ragland PC, eds (Geol Soc Am Spec Pap 268), pp. 233-259.
13. Blackburn TJ, et al. (2013) Zircon U–Pb geochronology links the end-Triassic extinction with the Central Atlantic Magmatic Province. *Science* 340:941–945.
14. Torrence C, Compo GP (1998) A practical guide to wavelet analysis. *Bull Am Meteorol Soc* 79:61–78.
15. Guex J, et al. (2012) Geochronological constraints on post-extinction recovery of the ammonoids and carbon cycle perturbations during the Early Jurassic. *Palaeogeogr Palaeoclimatol Palaeoecol* 346:1–11
16. Kent DV, et al. (2018) Empirical evidence for stability of the 405 kyr Jupiter-Venus eccentricity cycle over hundreds of millions of years. *PNAS* /doi/10.1073/pnas.1800891115.

-
17. Reynolds DJ (1993) *Sedimentary basin evolution: tectonic and climatic interaction*. [Ph.D. thesis]: New York, New York, Columbia University, Department of Earth and Environmental Sciences, 215 p.
 18. Kent DV, Olsen PE, Witte WK (1995) Late Triassic-earliest Jurassic geomagnetic polarity sequence and paleolatitudes from drill cores in the Newark rift basin, eastern North America. *J Geophys Res* 100:14965–14998.
 19. Kent DV, Olsen PE (1999) Astronomically tuned geomagnetic polarity time scale for the Late Triassic. *J Geophys Res* 104:12,831-12,841.
 20. Laskar J, Fienga A, Gastineau M, Manche H (2011) La2010: A new orbital solution for the long-term motion of the Earth. *Astron Astrophys* 532:81–15.
 21. Olsen PE, Kent DV (1999) Long-period Milankovitch cycles from the Late Triassic and Early Jurassic of eastern North America and their implications for the calibration of the Early Mesozoic time-scale and the long-term behaviour of the planets. *Philos Trans R Soc Lond A* 357:1761–1786.
 22. Laskar J et al. (2004) A long-term numerical solution for the insolation quantities of the Earth. *Astron Astrophys* 428(1):261-285.
 23. De Vleeschouwer D, et al. (2017) Alternating Southern and Northern Hemisphere climate response to astronomical forcing during the past 35 m.y. *Geology* 45(4):375-378.
 24. Laskar J (1990) The chaotic motion of the Solar System : a numerical estimate of the size of the chaotic zones. *Icarus* 88, 266-291.
 25. Laskar J (2005) Frequency Map analysis and quasi periodic decompositions, in *Hamiltonian systems and Fourier analysis*, Benest et al., eds, Taylor and Francis.
 26. Laskar J (1993) Frequency analysis for multi-dimensional systems. *Global dynamics and diffusion, Physica D* 67:257-281.
 27. Olsen PE (1986) A 40-million-year lake record of early Mesozoic climatic forcing. *Science* 234:842-848.
 28. Laskar J (1989) A numerical experiment on the chaotic behaviour of the Solar System. *Nature*, 338:237-238.
 29. Pälike H, Laskar J, Shackleton N (2004) Geologic constraints on the chaotic diffusion of the solar system. *Geology* 32(11):929–93a.
 30. Ma C, Meyers SR, Sageman BB (2017) Theory of chaotic orbital variations confirmed by Cretaceous geological evidence. *Nature* 542(7642):468–470.
 31. Laskar J, Gastineau M, Delisle J-B, Farres A, Fienga A (2011) Strong chaos induced by close encounters with Ceres and Vesta. *Astron Astrophys* 532:L4.
 32. The National Map Viewer (USGS): <https://nationalmap.gov/elevation.html>